

Models of J/Ψ photo-production reactions on the nucleon

T.-S. H. Lee^{a,1}, S. Sakinah^{b,2}, Yongseok Oh^{c,2,3}

¹Physics Division, Argonne National Laboratory, Argonne, Illinois 60439, USA

²Department of Physics, Kyungpook National University, Daegu 41566, Korea

³Asia Pacific Center for Theoretical Physics, Pohang, Gyeongbuk 37673, Korea

Received: date / Accepted: date

Abstract The J/Ψ photo-production reactions on the nucleon can provide information on the roles of gluons in determining the J/Ψ -nucleon (J/Ψ -N) interactions and the structure of the nucleon. The information on the J/Ψ -N interactions is needed to test lattice QCD (LQCD) calculations and to understand the nucleon resonances such as $N^*(P_c)$ recently reported by the LHCb Collaboration. In addition, it is also needed to investigate the production of nuclei with hidden charms and to extract the gluon distributions in nuclei. The main purpose of this article is to review six reaction models of $\gamma + p \rightarrow J/\Psi + p$ reactions which have been and can be applied to analyze the data from Thomas Jefferson National Accelerator Facility (JLab). The formulae for each model are given and used to obtain the results to show the extent to which the available data can be described. The models presented include the Pomeron-exchange model of Donnachie and Landshoff (*Pom*-DL) and its extensions to include J/Ψ -N potentials extracted from LQCD (*Pom*-pot) and to also use the constituent quark model (CQM) to account for the quark substructure of J/Ψ (*Pom*-CQM). The other three models are developed from applying the perturbative QCD approach to calculate the two-gluon exchange using the generalized parton distribution (GPD) of the nucleon (*GPD*-based), two- and three-gluon exchanges using the parton distribution of the nucleon ($2g + 3g$), and the exchanges of scalar (0^{++}) and tensor (2^{++}) glueballs within the holographic formulation (*holog*). The results of investigating the excitation of the nucleon resonances $N^*(P_c)$ in the $\gamma + p \rightarrow J/\Psi + p$ reactions are also given. We demonstrate that the differences between these six models can be unambiguously distinguished and the N^* can be better studied by using the forthcoming JLab data at large $|t|$ and at

energies very near the J/Ψ production threshold. Possible improvements of the considered models are discussed.

1 Introduction

One of the important subjects in Quantum Chromodynamics (QCD) is to understand the roles of gluons (g) in determining the structure of hadrons and hadron-hadron interactions. The progress in this direction can be made by investigating the interactions between the nucleon and the quark-antiquark ($q\bar{q}$) systems which do not share the same up (u) and down (d) quarks with the nucleon. The leading interaction between the nucleon (N) and the vector meson J/Ψ , which is a charm-anticharm ($c\bar{c}$) system with spin-parity $J^\pi = 1^-$, is the two-gluon exchange mechanism, as illustrated in Fig. 1. Higher order multi-gluon exchange effects can not be neglected in the non-perturbative region. The J/Ψ -N interaction can be estimated by using continuum and lattice studies at low energies and the heavy quark effective field theory and perturbative QCD (PQCD) at high energies. Alternatively, one can extract it from the data of J/Ψ photo-production reactions within appropriate reaction models. The information on the J/Ψ -N interaction is needed to understand the nucleon resonances $N^*(P_c)$ reported by the LHCb collaboration [1–4]. It is also needed to extract the gluonic distributions in nuclei, and to study the existence of nuclei with hidden charms [5–9].

The data of $\gamma + p \rightarrow J/\Psi + p$ reactions will be extensive and precise from Jefferson Laboratory (JLab) with 12 GeV upgrade in the near future [10–13]. The purpose of this paper is to review six reaction models which have been applied to investigate the first published JLab data [10], and can be used to analyze the forthcoming data. We will present formulas which are used to obtain the results presented in this paper for examining the extent to which the available data

^ae-mail: tshlee@anl.gov

^bssakinahf@gmail.com

^ce-mail: yohphy@knu.ac.kr

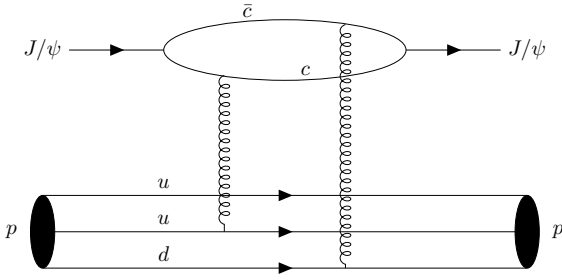


Fig. 1 One of the possible leading two-gluon exchange mechanisms of $\gamma + p \rightarrow J/\Psi + p$ reaction within QCD.

can be described by each model. Predictions will be presented for future experimental tests. In this section we will briefly describe the essential ingredients of these six models. The details are then given in the rest of the paper.

The study of photo-production of vector mesons (V) at high energies has a long history [14–16] with extensive data sets [17, 18]. A major advance was made by Donnachie and Landshoff [19–22] (DL) who demonstrated that the data of $\gamma + p \rightarrow V + p$ reactions at high energies can be described very well by using the Vector Meson Dominance (VMD) assumption [23–26] and the Pomeron-exchange mechanism within the Regge phenomenology [14, 15]. The connection of the DL model to QCD was qualitatively justified in some investigations [27–29] which attempted to relate the Pomeron-exchange to the gluon-exchange. In this approach, the incoming photon is converted into a vector meson V which is then scattered from the nucleon by the Pomeron-exchange between quarks in two hadrons, as illustrated in the upper part of Fig. 2. The main assumption of the DL model is the Pomeron-photon analogy [30, 31] that Pomerons interact with quarks like $C = +$ isoscalar photons and the usual factorization approximation can be used to simplify the loop-integration over quark wavefunctions of hadrons. Thus the emission or absorption of a Pomeron by a hadron can be calculated by using the electromagnetic form factors of hadrons, such as $F_1(t)$ of the nucleon. As illustrated in the lower part of Fig. 2, the amplitudes for $\gamma + p \rightarrow V + p$ within the DL model can be written schematically as

$$t^{\text{Pom}} \sim \left[\frac{e}{f_V} F_V(t) \right] \times G_P(s, t) \times F_1(t), \quad (1)$$

where f_V is determined by the width of $V \rightarrow e^+e^-$ decay using the VMD assumption, s and t are the usual Mandelstam variables, $F_V(t)$ is the form factor for V , and $G_P(t, s)$ is the Pomeron propagator of the Regge phenomenology. The model defined by Eq. (1) will be called *Pom-DL* model in this paper.

With the parameters determined by fitting [9, 32–34] the total cross section data of Refs. [17, 35–37] of $\gamma + p \rightarrow J/\Psi + p$ up to invariant mass $W = 300$ GeV, it was found [33] that the *Pom-DL* model can not describe the JLab data at $W < 7$ GeV. This is not unexpected because the J/Ψ -N in-

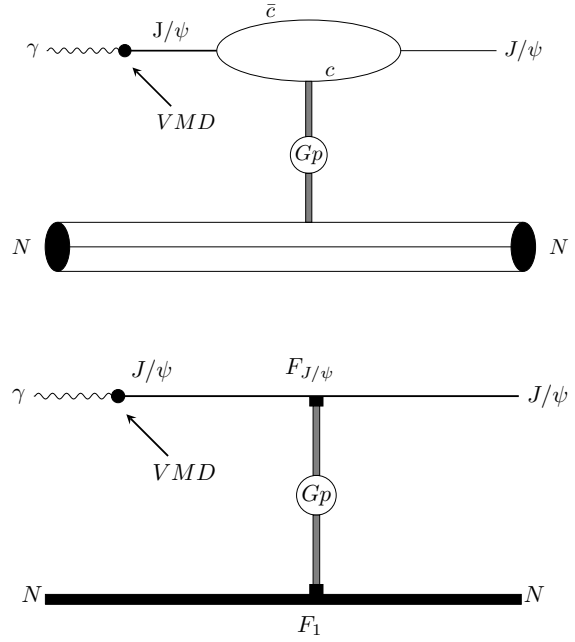


Fig. 2 Pomeron-exchange model of Donnachie and Landshoff (*Pom-DL*). Upper: Pomeron-exchange between quarks in J/Ψ and nucleon, Lower: Pomeron-exchange amplitude Eq. (1) resulted from assuming the Pomeron-photon analogy and using the factorization approximation.

teractions calculated by using the Pomeron-photon analogy is only part of possible gluon-exchange mechanisms. In the near threshold energy region where the relative velocity of the outgoing J/Ψ -N is not large and the higher order multi-gluon exchanges can not be neglected. In addition, the $J/\Psi + N \rightarrow J/\Psi + N$ transition amplitude $t_{J/\Psi N, J/\Psi N}(k, q, W)$ near threshold is far off-shell; for example, at $W = (m_N + m_{J/\Psi}) + 0.5$ GeV, the incoming γN relative momentum is $q = 0.8$ GeV which is much larger than the outgoing J/Ψ -N relative momentum $k = 0.1$ GeV in the CM system. Hence the Regge phenomenology, which is based on the on-shell formulation, is not directly applicable for describing $J/\Psi + N \rightarrow J/\Psi + N$ in the near threshold energy region.

An obvious next step [33] to improve the *Pom-DL* model is to add a J/Ψ -N scattering amplitude generated from a J/Ψ -N potential $v_{J/\Psi N, J/\Psi N}$ which can be interpreted as the multi-gluon exchange mechanisms. By also using the VMD assumption, it gives the amplitude, illustrated in the upper part of Fig. 3, which is of the following form,

$$t^{\text{pot}} = \frac{e m_{J/\Psi}^2}{f_{J/\Psi}} \frac{1}{q^2 - m_{J/\Psi}^2} t_{J/\Psi N, J/\Psi N}, \quad (2)$$

where $m_{J/\Psi}$ is the mass of J/Ψ , and the J/Ψ -N scattering amplitude is defined by the following Lippmann-Schwinger equation:

$$t_{J/\Psi N, J/\Psi N} = v_{J/\Psi N, J/\Psi N} + v_{J/\Psi N, J/\Psi N} G_{J/\Psi N}(W) t_{J/\Psi N, J/\Psi N}. \quad (3)$$

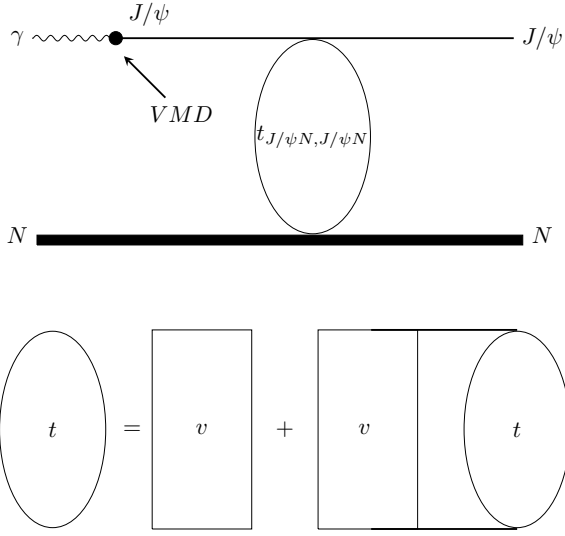


Fig. 3 *Pom*-pot model. Upper: The amplitude of Eq. (2). Lower: J/Ψ - N scattering equation (3). Here, v and t stand for $v_{J/\Psi N, J/\Psi N}$ and $t_{J/\Psi N, J/\Psi N}$, respectively.

Here, $G_{J/\Psi N}(W)$ is the propagator of the J/Ψ - N system. Eq. (3) is illustrated in the lower part of Fig. 3. Adding t^{pot} to the *Pom*-DL amplitude, we then obtain a *Pom*-pot model defined by the following amplitude

$$t^{\text{Pom+pot}} = t^{\text{Pom}} + t^{\text{pot}}. \quad (4)$$

The results from *Pom*-pot model depend on the choice of $v_{J/\Psi N, J/\Psi N}$ in solving Eq. (3). Several attempts had been made to determine $v_{J/\Psi N, J/\Psi N}$. An important step was taken by Peskin [38] who applied the operator product expansion to evaluate the strength of the color field emitted by heavy $q\bar{q}$ systems, and suggested [39] that the van der Waals force induced by the color field of J/Ψ on nucleons can generate an attractive short-range J/Ψ - N interaction. The results of Peskin were used by Luke, Manohar, and Savage [40] to predict, using the effective field theory method, the J/Ψ - N forward scattering amplitude which was then used to get an estimation that J/Ψ can have a few MeV/nucleon attraction in nuclear matter. The J/Ψ - N forward scattering amplitude of Ref. [40] was further investigated by Brodsky and Miller [41] to derive a J/Ψ - N potential which gives a J/Ψ - N scattering length of -0.24 fm. The result of Peskin was also used by Kaidalov and Volkovitsky [42], who differed from Ref. [41] in evaluating the gluon content in the nucleon, to give a much smaller scattering length of -0.05 fm.

In LQCD calculations using the approach of Refs. [43, 44], Kawanai and Sasaki [45, 46] obtained an attractive J/Ψ - N potential of the Yukawa form $v_{J/\Psi N, J/\Psi N} = -\alpha e^{-\mu r}/r$ with $\alpha = 0.1$ and $\mu = 0.6$ GeV, which gives a scattering length of -0.09 fm. Using the potential $v_{J/\Psi N, J/\Psi N}(r)$ extracted from this LQCD calculation, the *Pom*-pot model was used in Ref. [33] to fit the JLab data by including a reduction of the VMD coupling constant $1/f_{J/\Psi}$ by a factor of about

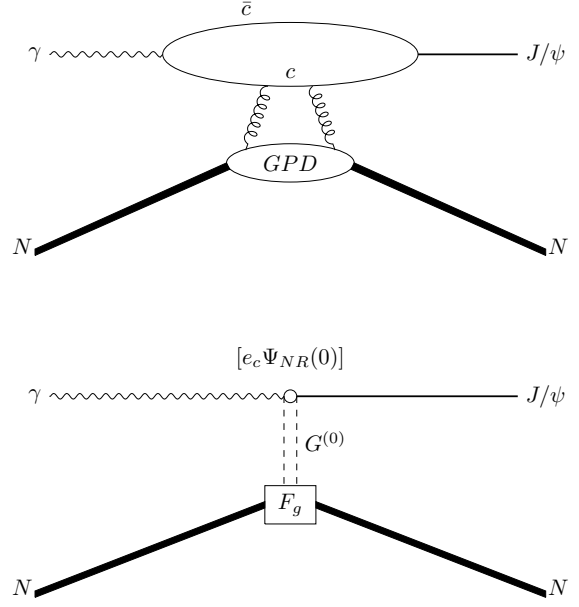


Fig. 4 *GPD*-based model. Upper: One of the four two-gluon exchange diagrams of Eq. (5). Lower: The amplitude of Eq. (6).

0.4–0.7. The need of such a correction on the VMD coupling constant is consistent with the earlier study of ρ photo-production [21]. It is also justified since the VMD coupling constant is determined by the $J/\Psi \rightarrow \gamma \rightarrow e^+e^-$ decay width at $q^2 = m_{J/\Psi}^2 \sim 9$ GeV² which is far from $q^2 = 0$ of the $\gamma + p \rightarrow J/\Psi + p$ reaction. Furthermore, the use of VMD for J/Ψ is questionable as discussed in Ref. [55]. Thus, the phenomenological procedure of adjusting the off-shell factor $1/f_{J/\Psi}$ makes the *Pom*-pot model uncertain in testing the LQCD calculations of J/Ψ - N potentials. Nevertheless, the *Pom*-pot model is the only model which fits the data from threshold to very high energy $W = 300$ GeV and therefore can be applied to use the data of J/Ψ photo-production on nuclei to study the gluonic distribution in nuclei and the existence of nuclei with hidden charms [5–9].

The models described above are for analyzing the data from threshold to very high energies up to $W = 300$ GeV. Focusing on the near threshold region $W \leq 7$ GeV, two models based on PQCD have been developed to describe the JLab data. Both models assume that the incoming photon fluctuates into a $c\bar{c}$ pair which is then scattered from the nucleon by gluon-exchange mechanisms.

The model of Ref. [47] starts with the two-gluon-exchange amplitude which is illustrated in the upper part of Fig. 4 and has the following form [48]

$$\begin{aligned} & t_{J/\Psi N, \gamma N}(P'K; Pq) \\ &= (ig)^2 \int \frac{d^4k d^4l}{(2\pi)^8} \langle P' | A^\mu(-l - \frac{\Delta}{2}) A^\nu(l - \frac{\Delta}{2}) | P \rangle \\ & \times \text{Tr} \left[\sum_{n=a}^d I_{\mu\nu}^n(K, k, l, \Delta, \varepsilon) \Psi(K, k) \right], \end{aligned} \quad (5)$$

where P and P' are the momenta of the initial and final nucleons, q the incident photon momentum, ε the photon polarization vector, K the final J/Ψ momentum, $\Delta \equiv P' - P$, A^μ the gluon field, $\Psi(K, k)$ the wavefunction of $c\bar{c}$ in J/Ψ , and $I_{\mu\nu}^a(K, k, l, \Delta, \varepsilon)$ the propagators of quarks in J/Ψ . The above expression can be simplified by using the heavy quark expansion in $1/m_{J/\Psi}$ and the non-relativistic limit of $\Psi(K, k)$. The amplitude is then reduced into a form related to the moment expansion of Generalized Parton Distribution (GPD). By keeping only the $n = 0$ moment, the cross section is then determined by a gluonic form factor of the nucleon and the non-relativistic wavefunction $\phi_{NR}(0)$ of J/Ψ at relative distance $r = 0$ of two quarks. The resulting amplitude is illustrated in the lower part of Fig. 4. The differential cross section can then be written as

$$\frac{d\sigma}{dt} = \frac{\alpha_{EM} e_c^2}{4(W^2 - m_N^2)^2} \frac{(16\pi\alpha_S)^2}{3m_{J/\Psi}^3} |\phi_{NR}(0)|^2 |G^{(0)}(t, \xi)|^2, \quad (6)$$

where $\alpha_{EM} = e^2/(4\pi) = 1/137$, $e_c = \frac{2}{3}e$, α_S is a QCD coupling constant, and $G^{(0)}(t, \xi)$ is the $n = 0$ moment of GPD defined by

$$G^{(0)}(t, \xi) = \frac{1}{\xi^2} \int_{-1}^{+1} dx F_g(x, \xi, t). \quad (7)$$

Here the skewness ξ is defined by $\xi = \frac{P^+ - P'^+}{P^+ + P'^+}$ with $P^+ = \frac{1}{2}(P^0 + P^3)$, and $F_g(x, \xi, t)$ is the gluon GPD of the nucleon. The parameters of $G^{(0)}(t, \xi)$ had been determined [49] by using LQCD, but were adjusted to fit the JLab data. The model defined by Eqs. (6) and (7) will be called *GPD-based model* in this paper.

The PQCD model of Ref. [50], applied in Ref. [10] to fit the JLab data, assumes that the $c\bar{c}$ scattered from the valance quarks with fraction of momentum $x \sim 1$ of the target nucleus. For the nucleon target, this model has two- and three-gluon exchange processes, as illustrated in Fig. 5. As discussed in Ref. [51], this implies that the production rate behaves near $x \rightarrow 1$ as $(1-x)^{2n_s}$, where n_s is the number of spectators. They also follow Ref. [52] to assume that the probability that a quark in the proton of radius R is found within the transverse distance $1/M_{c\bar{c}}$ of $c\bar{c}$ from proton is $1/(R^2 M_{c\bar{c}}^2)$, where $M_{c\bar{c}}$ is the mass of $c\bar{c}$. For exclusive J/Ψ production, a form factor $F_{ng}(t)$ is needed to describe how the scattered quarks combine with the spectator quarks to form a proton. They then obtain

$$\frac{d\sigma_{2g}}{dt} = N_{2g} \frac{(1-x)^2}{R^2 M_{c\bar{c}}^2} F_{2g}^2(t) (s - m_p^2), \quad (8)$$

$$\frac{d\sigma_{3g}}{dt} = N_{3g} \frac{(1-x)^0}{R^4 M_{c\bar{c}}^4} F_{3g}^2(t) (s - m_p^2), \quad (9)$$

where the factor $(s - m_p^2)$ is from the coupling of photon to $c\bar{c}$. It is rather uncertain to estimate x and they assumed

$$x = (2m_p M_{c\bar{c}} + M_{c\bar{c}}^2)/(s - m_p^2), \quad (10)$$

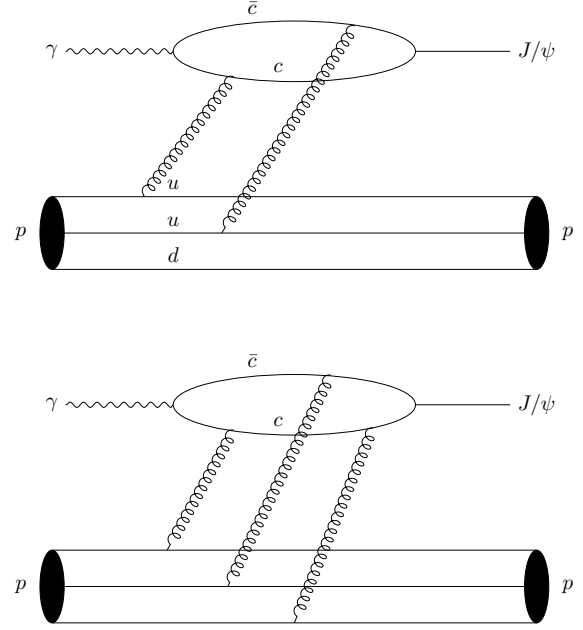


Fig. 5 The $2g + 3g$ model. Upper: two-gluon exchange, Lower: three-gluon exchange.

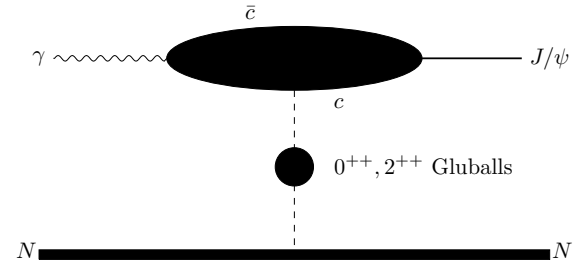


Fig. 6 The holographic model.

where $s = E_{cm}^2$ with E_{cm} being the total energy in the center of mass frame. The form factors $F_{2g}(t)$ and $F_{3g}(t)$ are unknown and must be determined from experiments. Using rather scarce data of t -dependence of $d\sigma/dt$ near threshold, they set $F_{2g}^2(t) = F_{3g}^2(t) = \exp(1.13t)$, where t is in the units of GeV^2 . The constants N_{2g} and N_{3g} are then determined from fitting the total cross section data of $\gamma + p \rightarrow J/\Psi + p$ reactions. The model defined by Eqs. (8) and (9) will be called $2g + 3g$ model in this paper.

We will also give formula of the model of Refs. [53, 54] based on the holographic QCD. This model assumes that the J/Ψ photo-production is due to the exchanges of tensor (2^{++}) and scalar (0^{++}) glueballs, as illustrated in Fig. 6. This model will be called *Holog model* in this paper.

The sixth model we will present is aimed at testing the J/Ψ -N potentials extracted from LQCD calculations. It is obtained by removing the VMD assumption, which is questionable [55] for J/Ψ , in the *Pom-pot* model described above. If we further assume that the $c\bar{c}$ -N interaction can be defined by a quark-N potential v_{cN} , then the $\gamma + N \rightarrow J/\Psi + N$ and

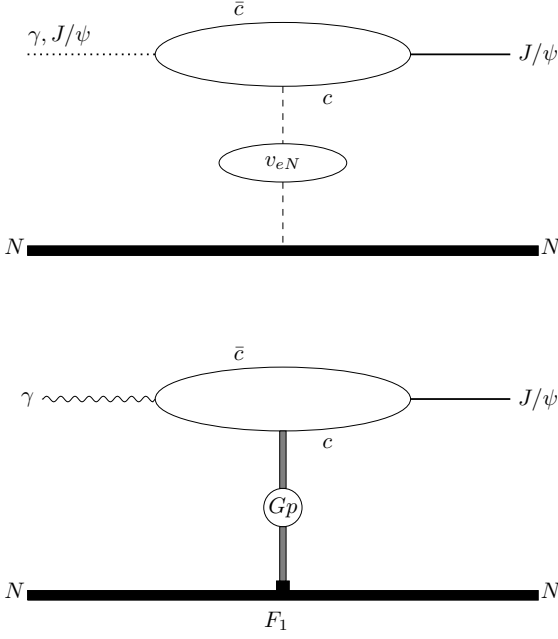


Fig. 7 Models with $c\bar{c}$ -loop mechanisms. Upper: calculated from quark-nucleon potential (v_{cN}), Lower: calculated from Pomeron-exchange mechanism.

$J/\Psi + N \rightarrow J/\Psi + N$ amplitudes in t^{pot} of Eqs. (2) and (3) are defined by $c\bar{c}$ -loop mechanisms, as illustrated in the upper part of Fig. 7. Similarly, the Pomeron-exchange term t^{Pom} should also be defined by the same $c\bar{c}$ -loop mechanism, as illustrated in the lower part of Fig. 7. By using a hadron model [56, 57] based on Dyson-Schwinger equation (DSE) of QCD, such a quark-loop Pomeron-exchange model was explored in Refs. [58, 59]. It will be interesting to use the recent DSE models [60–67] to improve the results of Refs. [58, 59] and to also evaluate loop mechanisms with v_{cN} (upper part of Fig. 7) which is needed to describe the data near threshold.

Alternatively, one can use the constituent quark model (CQM) [68–70] to evaluate the $c\bar{c}$ -loops of Fig. 7. This approach is simpler in practice and is reasonable since CQM for the heavy quark systems, such as J/Ψ and Υ , has been well established [69]. In this paper, we will detail how such a CQM-based model, referred to as *Pom-CQM* model, can relate the J/Ψ potentials extracted from LQCD calculations to the J/Ψ photo-production data.

The N^* excitation in the J/Ψ photo-production has been studied in Ref. [32] within the dynamical formulation developed in Refs. [71–74]. In this Argonne-Osaka approach, the total amplitude including the excitation of N^* is of the following form:

$$T_{VN,\gamma N}(W) = t_{VN,\gamma N}(W) + t_{VN,\gamma N}^{N^*}(W), \quad (11)$$

where $t_{VN,\gamma N}$ can be generated from any of the models described above, and

$$t_{VN,\gamma N}^{N^*}(W) = \bar{F}_{N^*,VN}^+(W) \frac{1}{W - M_0^* - \Sigma(W)} \bar{F}_{N^*,\gamma N}(W), \quad (12)$$

where $\bar{F}_{N^*,MB}$ is the dressed $N^* \rightarrow MB$ vertex function, and $\Sigma(W)$ is the self-energy of the resonance with a bare mass M_0^* . The $VN \rightarrow VN$ scattering amplitudes are included in $\bar{F}_{N^*,VN}$ and $\Sigma(W)$, as required by the unitarity condition. The above dynamical formulation can be used to investigate whether $N^*(P_c)$ states are the meson-baryon molecules [75–78] or the compact pentaquark states [79–81]. We will present results from using Eqs. (11) and (12) to investigate the $N^*(P_b)$ reported in Ref. [4].

In Sec. 2, we briefly review the Regge phenomenology for explaining the Pomeron-exchange model of Donnachie and Landshoff (*Pom-DL*). The *Pom-pot* model obtained from extending the *Pom-DL* model to include J/Ψ -N potentials extracted from LQCD is presented in Sec. 3. The models based on GPD (*GPD-based*), two-gluon and three-gluon exchange ($2g + 3g$), and holographic approach (*Holog*) are presented in Sec. 4. The study of N^* excitation is given in Sec. 5. Section 6 is for presenting the *Pom-CQM* model. Predictions for future experimental tests are given in Sec. 7. In Sec. 8, we give a summary and discuss possible future developments.

2 Pomeron-exchange model

The Pomeron-exchange model of photo-production of vector mesons was developed within the Regge phenomenology. As can be seen from extensive literature [14–16], the Regge phenomenology cannot be derived rigorously from relativistic quantum field theory, although some understanding of Regge poles have been obtained in Ref. [82]. It was largely from the study [83–85] of potential scattering within the non-relativistic quantum mechanics and was simply extended to relativistic formulation [86–88] of scattering amplitudes. For our purposes, we give in Appendix A sufficiently self-contained explanations which are needed to develop the formulas of Pomeron-exchange models.

With the derivations given in Appendix A, we start with Eq. (A.19) for the amplitude $T(s, t)$ of the process $1(p_1) + 2(p_2) \rightarrow 3(p_3) + 4(p_4)$. By defining the usual Mandelstam variables as

$$s = (p_1 + p_2)^2, \quad (13)$$

$$t = (p_1 - p_3)^2, \quad (14)$$

we have

$$T(s, t) = \sum_n \beta_n^{13}(t) \beta_n^{24}(t) \frac{1 + s_n e^{-i\pi\alpha_n(t)}}{2 \sin[\pi\alpha_n(t)]} (\alpha_{1,n} s)^{\alpha_n(t)}, \quad (15)$$

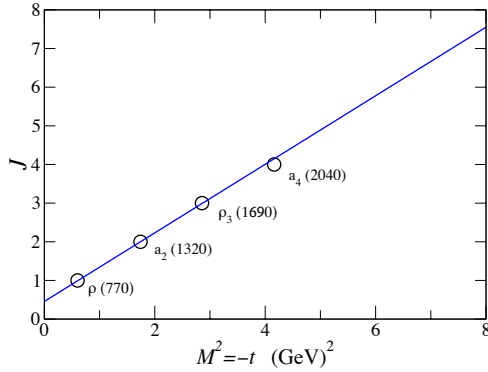


Fig. 8 The ρ trajectory determined by the masses of $\rho(760)$, $a_2(1320)$, $\rho_3(1690)$ and $a_4(2040)$.

where $s_n = +1$ (-1) corresponds to even (odd) parity exchanges, $\beta_n^{13}(t)$ and $\beta_n^{24}(t)$ characterize the hadron structure, and $\alpha_n(t) = \alpha_{0,n} + \alpha_{1,n}t$ defines the Regge trajectory n . We now note that the amplitude $T(s,t)$ has singularities in t defined by $\alpha_n(t) = \text{integers}$. It has the feature of the one-particle-exchange amplitude in the relativistic quantum field theory,

$$T(s,t) \sim \frac{1}{t - m^2}, \quad (16)$$

which has singularity at $t = m^2$. Thus the amplitude (15) can be interpreted as the exchange of particles with masses M_{L_n} defined by $\alpha_n(t = M_{L_n}^2) = L_n$ with L_n being the spin quantum number of the exchanged particle. This is an intuitively very attractive interpretation of the scattering amplitude (15). However, there exists no successful derivation of Eq. (15) from relativistic quantum field theory and the form factors $\beta_n^{13}(t)$ and $\beta_n^{24}(t)$ are determined experimentally or calculated from hadron models.

We now turn to explaining how the Pomeron-exchange is introduced in Regge phenomenology. It was from examining the total cross sections σ^{tot} defined by the amplitude of Eq. (15):

$$\begin{aligned} \sigma^{\text{tot}} &= \int dt \frac{d\sigma}{dt} \\ &= \int dt \left(\frac{1}{16\pi s^2} \right) |T(s,t)|^2. \end{aligned} \quad (17)$$

2.1 Hadron-hadron scattering

The approach based on Eqs. (15) and (17) had been applied [89–91] to investigate the hadron-hadron scattering. The first step is to use the existing particle spectra to determine the Regge trajectories. It was found that the trajectories for $n = \pi, \rho, \dots$ can be written as

$$\alpha_n(t) = \alpha_{0,n} + \alpha_{1,n}t, \quad (18)$$

where

$$\alpha_{0,n} < 1. \quad (19)$$

An example for the ρ trajectory is illustrated in Fig. 8 with $\alpha_0 = 0.456$ and $\alpha_1 = 0.887 \text{ GeV}^{-2}$. If these trajectories are included in calculating the total cross section (17), we then find that at very large s , only one trajectory n_s dominates. Since $\alpha_{0,n} < 1$, Eq. (17) leads to

$$\sigma^{\text{tot}}(s) \sim s^{2(\alpha_{0,n_s}-1)} = s^{-m}; \quad m > 0. \quad (20)$$

Eq. (20) contradicts with the experimental data that the total cross sections $\sigma^{\text{tot}}(s)$ of all hadron-hadron scattering increase with s as s becomes large. It is also in disagreement with the Pomernchuk theorem [92]. A way to solve this problem is to add a trajectory with $\alpha_{0,P} > 1$ which does not correspond to any known particle spectrum. This trajectory was called Pomeron trajectory with the exchanged particles carrying the quantum number of “vacuum”. Within QCD, it is natural to identify the Pomeron-exchange with the gluon-exchange, as investigated in Refs. [27–29]. Accordingly, the the form factors $\beta_P^{13}(t)$ and $\beta_P^{24}(t)$ in Eq. (A.19) for the Pomeron trajectory can be interpreted as the form factors due to the Pomeron-quark coupling.

An important step was taken by Donnachie and Landshoff [19] who demonstrated that very extensive hadron-hadron scattering data at high s can be described very well by including only the Pomeron trajectory and assuming

1. Pomeron-photon analogy [30, 31]: Pomeron couples with a quark in hadron like a photon and carries $s_P = +$ signature in Eq. (15) to give it even C -parity.
2. The factorization approximation can be used to write the Pomeron-hadron form factor as

$$\beta_P^{hh}(t) = \sum_q \beta_q F_h(t), \quad (21)$$

where $F_h(t)$ is the electromagnetic form factor of the hadron h , and β_q is the Pomeron-quark coupling constant. For the nucleon $h = N$, $F_N(t) = F_1(t)$ is the well determined Dirac form factor.

With the above assumptions, Eq. (15) for $A + B \rightarrow A + B$ scattering with even parity exchange $n_s = +1$ at high s then becomes

$$\begin{aligned} T(s,t) &= [\beta_{q_A} n_A F_A(t)] [\beta_{q_B} n_B F_B(t)] \frac{1 + e^{-i\pi\alpha_P(t)}}{2 \sin(\pi\alpha_P(t))} \\ &\quad \times (\alpha_{1,P} s)^{\alpha_P(t)} \\ &= [\beta_{q_A} n_A F_A(t)] [\beta_{q_B} n_B F_B(t)] \frac{e^{-i\frac{\pi}{2}(\alpha_P(t)-1)}}{2 \sin(\frac{\pi}{2}\alpha_P(t))} \\ &\quad \times (\alpha_{1,P} s)^{\alpha_P(t)}, \end{aligned} \quad (22)$$

where n_h is the number of quarks in the hadron h ; $n_N = 3$ for the nucleon, $n_\pi = 2$ for the pion etc., β_{q_A} is the quark-Pomeron coupling constant in hadron A ; $\beta_{q_A} = \beta_{q_B} = \beta_u = \beta_d$ for πN and pp scattering.

Taking $F_1(t)$ and $F_\pi(t)$ extracted from the experimental data, Donnachie and Landshoff [19] demonstrated that the total cross sections and the differential cross section data of pp , $p\bar{p}$ and π^+p at small $|t|$ and high s can be described within 10% with the following parameters:

$$\alpha_p(t) = 1.08 + 0.25t, \quad (23)$$

$$\beta_u^2 = \beta_d^2 = 3.21 \text{ GeV}^{-2}, \quad (24)$$

where t is in the units of GeV^2 . The Pomeron-photon analogy had also been applied to get reasonably good description of diffractive dissociation reaction $e + A \rightarrow e + X$ with the assumption that the exchanged photon absorbed by one of the nucleons which is then elastically scattered from one of the other nucleon in the breakup system. The details can be found in Ref. [16]. We now turn to explaining how the Pomeron-exchange model of Donnachie and Landshoff can be applied to describe photoproduction of vector mesons.

2.2 Photo-production of vector mesons

To use the Pomeron-exchange amplitude defined by Eq. (22) to describe the photo-production of vector mesons, one assumes that the incoming photon is converted into a vector meson V by using the Vector Meson Dominance (VMD) model [23–26] defined by

$$L_{\text{VMD}} = \frac{em_V^2}{f_V} \phi_V^\mu(x) A_\mu(x), \quad (25)$$

where $\phi_V(x)$ and $A_\mu(x)$ are the field operators for the vector meson V and the photon, respectively. The coupling constant f_V is traditionally determined by using Eq. (25) to calculate the $V \rightarrow \gamma \rightarrow e^+e^-$ decay width:

$$\Gamma_{V \rightarrow e^+e^-} = \frac{1}{3} \alpha_{em}^2 m_V \frac{4\pi}{f_V^2}. \quad (26)$$

With the Lagrangian of Eq. (25), one can extend the $V + N \rightarrow V + N$ amplitude, defined by Eq. (22), to describe $\gamma + N \rightarrow V + N$. The resulting *Pom*-DL model is illustrated in the lower part of Fig. 2. The *Pom*-DL model had been applied in Refs. [9, 32–34] to fit the total cross section data of $\gamma + p \rightarrow V + p$ with $V = \rho, \phi, J/\Psi, Y$. The formulas used in Refs. [9, 33], as given below, are used in the calculations presented in this paper.

We use the convention [93] that the plane-wave state, $|\mathbf{k}\rangle$, is normalized as $\langle \mathbf{k} | \mathbf{k}' \rangle = \delta(\mathbf{k} - \mathbf{k}')$ and the S -matrix is related to the scattering T -matrix by

$$S_{fi} = \delta_{fi} - 2\pi i \delta(E_i - E_f) T_{fi}. \quad (27)$$

In the center of mass (CM) frame, the differential cross section of vector meson (V) photo-production reaction, $\gamma(\mathbf{q}) +$

$N(-\mathbf{q}) \rightarrow V(\mathbf{k}) + N(-\mathbf{k})$, is calculated from

$$\begin{aligned} \frac{d\sigma_{VN,\gamma N}}{d\Omega}(W) &= \frac{(2\pi)^4}{q^2} \rho_{VN}(k) \rho_{\gamma N}(q) \\ &\times \frac{1}{4} \sum_{\lambda_V, m'_s} \sum_{\lambda_\gamma, m_s} |\langle \mathbf{k}, \lambda_V m'_s | T_{VN,\gamma N}(W) | \mathbf{q}, \lambda_\gamma m_s \rangle|^2, \end{aligned} \quad (28)$$

where m_s denotes the z -component of the nucleon spin, and λ_V and λ_γ are the helicities of vector meson V and photon γ , respectively, and

$$\rho_{VN}(k) = \frac{k E_V(k) E_N(k)}{W}, \quad (29)$$

$$\rho_{\gamma N}(q) = \frac{q^2 E_N(q)}{W}. \quad (30)$$

The magnitudes of $k = |\mathbf{k}|$ and $q = |\mathbf{q}|$ are defined by the invariant mass $W = q + E_N(q) = E_V(k) + E_N(k)$.

Within the *Pom*-DL model, the $\gamma + N \rightarrow V + N$ amplitude in Eq. (28) is

$$\langle \mathbf{k}, \lambda_V m'_s | T_{VN,\gamma N}(W) | \mathbf{q}, \lambda_\gamma m_s \rangle = \langle \mathbf{k}, \lambda_V m'_s | t^{\text{Pom}}(W) | \mathbf{q}, \lambda_\gamma m_s \rangle, \quad (31)$$

where

$$\begin{aligned} \langle \mathbf{k}, \lambda_V m'_s | t^{\text{Pom}}(W) | \mathbf{q}, \lambda_\gamma m_s \rangle &= \\ &\frac{1}{(2\pi)^3} \sqrt{\frac{m_N m_N}{4E_V(\mathbf{k}) E_N(\mathbf{p}_f) |\mathbf{q}| E_N(\mathbf{p}_i)}} \\ &\times [\bar{u}(p_f, m'_s) \varepsilon_\mu^*(k, \lambda_V) \mathcal{M}_\mathbb{P}^{\mu\nu}(k, p_f, q, p_i) \varepsilon_\nu(q, \lambda_\gamma) u(p_i, m_s)]. \end{aligned} \quad (32)$$

In the above equation, we have defined four-momenta as $k = (E_V(\mathbf{k}), \mathbf{k})$, $p_f = (E_N(\mathbf{k}), -\mathbf{k})$, $q_i = (q, \mathbf{q})$, $p_i = (E_N(\mathbf{q}), -\mathbf{q})$, and $\varepsilon_\nu(q, \lambda_\gamma)$ is the polarization vector of photon, $\varepsilon_\nu(k, \lambda_V)$ the polarization vector of vector meson V , and $u(p, m_s)$ is the nucleon spinor with the normalization $\bar{u}(p, m_s) u(p, m'_s) = \delta_{m_s, m'_s}$. The Pomeron-exchange amplitude $\mathcal{M}_\mathbb{P}^{\mu\nu}(k, p_f, q, p_i)$ can be written as

$$\mathcal{M}_\mathbb{P}^{\mu\nu}(k, p_f, q, p_i) = G_\mathbb{P}(s, t) \mathcal{T}_\mathbb{P}^{\mu\nu}(k, p_f, q, p_i) \quad (33)$$

with

$$\begin{aligned} \mathcal{T}_\mathbb{P}^{\mu\nu}(q, p, q', p') &= i2 \frac{em_V^2}{f_V} [2\beta_{qV} F_V(t)] [3\beta_{u/d} F_1(t)] \\ &\times \{qg^{\mu\nu} - q^\mu \gamma^\nu\}, \end{aligned} \quad (34)$$

where M_V is the mass for the vector meson, and $f_V = 5.3, 15.2, 13.4, 11.2, 40.53$ for $V = \rho, \omega, \phi, J/\Psi, Y$. The parameters β_{qV} ($\beta_{u/d}$) define the coupling of the Pomeron with the quark q_V (u or d) in the vector meson V (nucleon N). In Eq. (34) a form factor for the Pomeron-vector meson vertex is also introduced with

$$F_V(t) = \frac{1}{m_V^2 - t} \left(\frac{2\mu_0^2}{2\mu_0^2 + m_V^2 - t} \right), \quad (35)$$

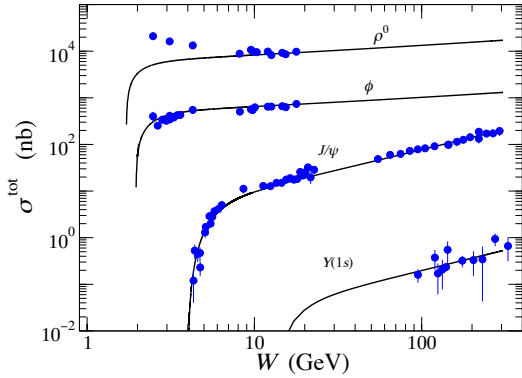


Fig. 9 Fits to the data of the total cross sections (σ^{tot}) of photo-production of ρ^0 , ϕ , J/Ψ and $\Upsilon(1s)$ on the proton target. The solid curves are calculated from using the *Pom-DL* model. Data are from Refs. [17, 35–37, 95–106].

where $t = (q - k)^2 = (p_f - p_i)^2$. By using the Pomeron-photon analogy, the form factor for the Pomeron-nucleon vertex is defined by the isoscalar electromagnetic form factor of the nucleon as

$$F_1(t) = \frac{4m_N^2 - 2.8t}{(4m_N^2 - t)(1 - t/0.71)^2}. \quad (36)$$

Here t is in the unit of GeV^2 , and m_N is the proton mass.

The crucial ingredient of Regge phenomenology is the propagator $G_{\mathbb{P}}$ of the Pomeron in Eq. (33). Following Eq. (22) and using $\sin[\frac{\pi}{2}\alpha_P(t)] \sim 1$ for $\alpha_P(t) \sim 1$ in the small $|t|$ region, it is of the following form:

$$G_{\mathbb{P}} = \left(\frac{s}{s_0}\right)^{\alpha_P(t)-1} \exp\left\{-\frac{i\pi}{2}[\alpha_P(t)-1]\right\}, \quad (37)$$

where $s = (q + p_i)^2 = W^2$, $\alpha_P(t) = \alpha_0 + \alpha'_P t$, and $s_0 = 1/\alpha'_P$.

The amplitude of the *Pom-DL* model, as defined above, has the parameters: the quark-Pomeron coupling constants β_q for $q = u/d, s, c, b$, μ_0 for the form factor $F_V(t)$ of the vector meson V , and α_0 and α'_P for the Regge trajectory $\alpha_P(t)$. The nucleon form factor $F_1(t)$ is given in Eq. (36) and we set $s_0 = 1/\alpha'_P = 0.25$ GeV from Donnachie and Landshoff. By fitting the data of ρ^0 , ω , ϕ photo-production [94], we have determined: $\mu_0 = 1.1$ GeV^2 , $\beta_{u/d} = 2.07$ GeV^{-1} , $\beta_s = 1.38$ GeV^{-1} , $\alpha_0 = 1.08$ for ρ and ω , $\alpha_0 = 1.12$ for ϕ . For the heavy quark systems, we find that with the same μ_0^2 , $\beta_{u/d}$, and α'_P , the J/Ψ and Υ photo-production data can be fitted by setting $\beta_c = 0.32$ GeV^{-1} and $\beta_b = 0.45$ GeV^{-1} , and choosing a larger $\alpha_0 = 1.25$.

In Fig. 9, we see that the data for the ϕ , J/Ψ , and Υ production can be described very well by the *Pom-DL* model. On the other hand, the ρ photo-production data at low energies clearly need other mechanisms such as the meson-exchange mechanisms illustrated in Refs. [58, 59] or the

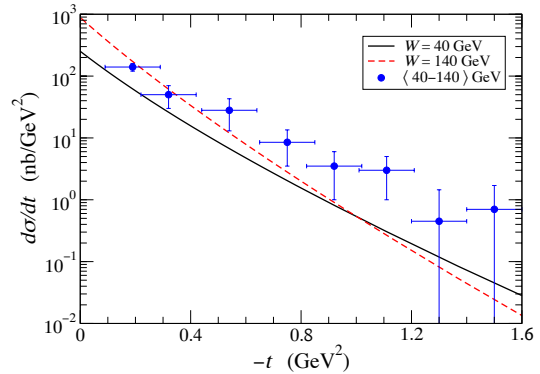
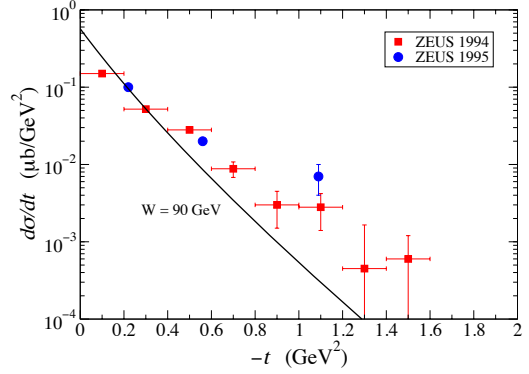


Fig. 10 Differential cross sections from the *Pom-DL* model are compared with ZEUS data [17, 35–37]. Upper: at $W = 90$ GeV; Lower: at $W = 40$ GeV (solid curve) and 140 GeV (dashed curve), data are from averaging the data in the range of $W = 40$ - 140 GeV.

mechanisms due to the a_2 and f_2 Regge trajectories as included in Refs. [21, 107]. It appears that the slope parameter α_0 for the energy-dependence of the diffractive production of heavy quarks (c and b) is rather different from that for light quarks (u , d , s). This was interpreted [22] as the presence of second Pomeron. As with much of Pomeron phenomenology, it will be good to understand this observation within QCD.

In Fig. 10, we show that the predicted differential cross sections at $W = 40$ - 140 GeV are consistent with the data (averaged over the cross sections in a range of W), while some refinements of the model are needed to fit data at large $-t$. It is worthwhile to use the *Pom-DL* model to illustrate that in the near threshold energy region $W \lesssim 5$ GeV, the cross sections are from the large momentum-transfer region where the Regge phenomenology may not be applicable. This can be seen in Fig. 11. At the very near threshold $W = 4.075$ GeV, the momentum transfers are in the $-t > 1.4$ GeV^2 region. We thus expect that the *Pom-DL* model needs to be improved to fit the JLab data. This can be seen in Fig. 12

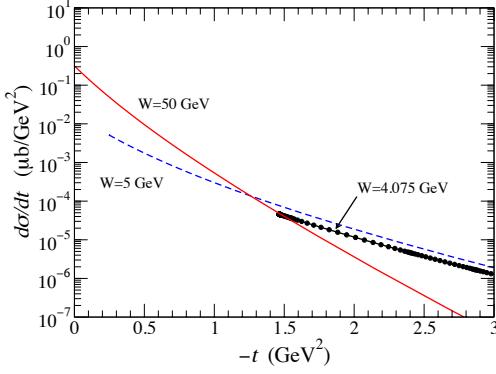


Fig. 11 Differential cross sections at $W = 4.075, 5, 50$ GeV calculated from the *Pom*-DL model.

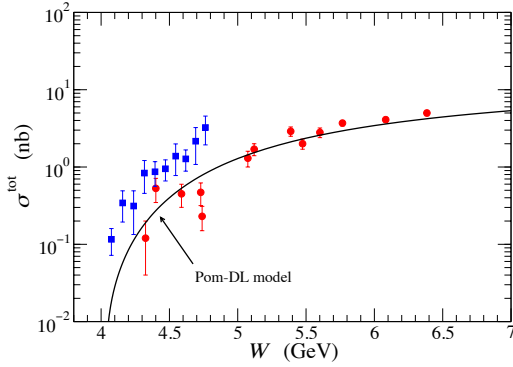


Fig. 12 Total cross sections calculated from the *Pom*-DL model are compared with the data. Solid squares are the JLab data [10].

where the predicted total cross sections are shown to be much smaller than the JLab data.

3 *Pom*-pot model

The results shown in Fig. 12 is not unexpected since the use of Pomeron-photon analogy only accounts for parts of gluon-exchange mechanisms which may not be the dominant mechanism in the near threshold region. Adding the non-perturbative multi-gluon exchange mechanisms as included in the J/Ψ -N potentials $v_{J/\Psi N, J/\Psi N}$ extracted from LQCD may solve the problem. By also using the VMD assumption, the amplitude (t^{pot}) due to a potential $v_{J/\Psi N, J/\Psi N}$ is illustrated in Fig. 3.

To proceed, we note that the VMD coupling constant $1/f_V$ is determined by the $J/\Psi \rightarrow \gamma \rightarrow e^+e^-$ decay at $q^2 = m_{J/\Psi}^2 \sim 9 \text{ GeV}^2$ which is far from $q^2 = 0$ for the photo-production process. It is therefore necessary to include an off-shell factor $F_{\text{off}}(q^2)$ with $F_{\text{off}}(m_V^2) = 1$ to correct this. This phenomenological procedure is needed since VMD for

J/Ψ is questionable, as recently claimed in Ref. [64]. The amplitude from extending the *Pom*-DL model to include the amplitude t^{pot} shown in Fig. 3 due to $v_{J/\Psi N, J/\Psi N}$ has the following form:

$$\langle \mathbf{k}, \lambda_V m'_s | T_{VN, \gamma N}(W) | \mathbf{q}, \lambda_\gamma m_s \rangle = \langle \mathbf{k}, \lambda_V m'_s | t^{\text{Pom}+\text{pot}}(W) | \mathbf{q}, \lambda_\gamma m_s \rangle \quad (38)$$

with

$$\langle \mathbf{k}, \lambda_V m'_s | t^{\text{Pom}+\text{pot}}(W) | \mathbf{q}, \lambda_\gamma m_s \rangle = \langle \mathbf{k}, \lambda_V m'_s | t^{\text{Pom}}(W) | \mathbf{q}, \lambda_\gamma m_s \rangle + \langle \mathbf{k}, \lambda_V m'_s | t^{\text{pot}}(W) | \mathbf{q}, \lambda_\gamma m_s \rangle, \quad (39)$$

where $\langle \mathbf{k}, \lambda_V m'_s | t^{\text{Pom}}(W) | \mathbf{q}, \lambda_\gamma m_s \rangle$ has been given in Eq. (32), and we follow the dynamical formulation of Refs. [71–74] to write

$$\begin{aligned} \langle \mathbf{k}, \lambda_V m'_s | t^{\text{pot}}(W) | \mathbf{q}, \lambda_\gamma m_s \rangle &= \langle \mathbf{k}, \lambda_V m'_s | t_{VN, VN}(W) | \mathbf{q}, \lambda_\gamma m_s \rangle \\ &\times \frac{1}{W - E_N(q) - E_V(q) + i\epsilon} \\ &\times \left[F_{\text{off}}(0) \frac{em_V^2}{f_V} \frac{1}{(2\pi)^{3/2}} \frac{1}{\sqrt{2q}} \frac{1}{\sqrt{2E_V(q)}} \right]. \quad (40) \end{aligned}$$

Here, the J/Ψ -N scattering amplitude $t_{VN, VN}(W)$ is calculated from potential $v_{VN, VN}$ by using the following Lippmann-Schwinger equation,

$$t_{VN, VN}(W) = v_{VN, VN} + v_{VN, VN} \frac{1}{W - H_0 + i\epsilon} t_{VN, VN}(W). \quad (41)$$

The above equation is solved in partial-wave representation. For a central potential, such as $v_{J/\Psi N, J/\Psi N} = v_0 \frac{-\alpha r}{r}$ extracted from LQCD [45], we have

$$\langle \mathbf{k}, m_V m_s | t_{VN, VN}(W) | \mathbf{k}', m'_V m'_s \rangle = \sum_{LM} Y_{LM}^*(\hat{k}) t_L(k, k', W) Y_{LM}(\hat{k}') \delta_{m_V, m'_V} \delta_{m_s, m'_s}. \quad (42)$$

The matrix element $t_L(k, k', W)$ is then from solving

$$\begin{aligned} t_L(k, k', W) &= v_L(k, k') \\ &+ \int q^2 dq v_L(k, q) \frac{1}{W - E_N(q) - E_V(q) + i\epsilon} \\ &\times t_L(q, k', W), \quad (43) \end{aligned}$$

where

$$v_L(k, k') = \frac{2}{\pi} \int r^2 dr j_L(kr) v_{VN, VN}(r) j_L(k'r). \quad (44)$$

The *Pom*-pot model has been applied in Ref. [33] by using $v_{J/\Psi N, J/\Psi N}$ extracted from the LQCD calculations of Refs. [45, 108]. As shown in Fig. 13, the LQCD data (solid circles) can be fitted by two sets of parameters: (1) $v_0 = -0.06$, $\alpha = 0.3 \text{ GeV}$ (pot-1), (2) $v_0 = -0.11$, $\alpha = 0.5 \text{ GeV}$ (pot-2). It is found that the JLab data can be fitted by choosing the off-shell factor $F_{\text{off}}(0) = 0.7$ (0.4) for pot-1 (pot-2). The results from using pot-1 are shown in Fig. 14. We see that the amplitude t^{pot} from $v_{J/\Psi N, J/\Psi N}$ interferes with t^{Pom} from the *Pom*-DL model to fit the JLab data in $W < 5 \text{ GeV}$ region, while the fits at higher energies are also improved.

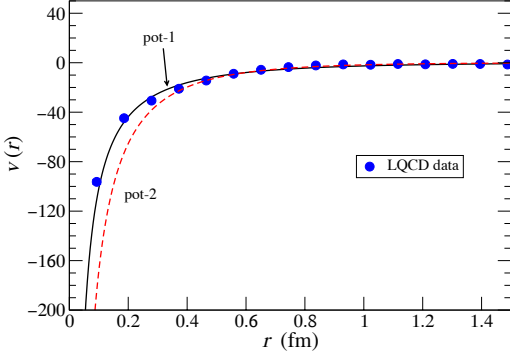


Fig. 13 The J/Ψ - N potential $v_{J/\Psi N, J/\Psi N}(r) = v_0 \frac{e^{-\alpha r}}{r}$ extracted from the LQCD calculations of Refs. [45, 108].

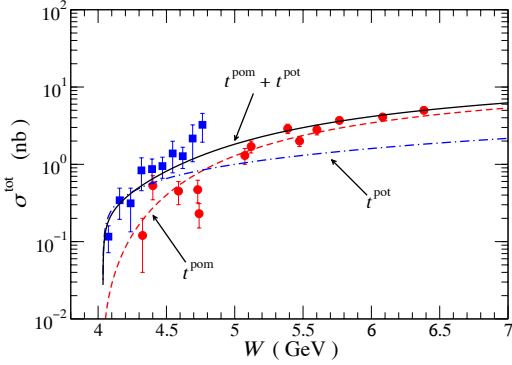
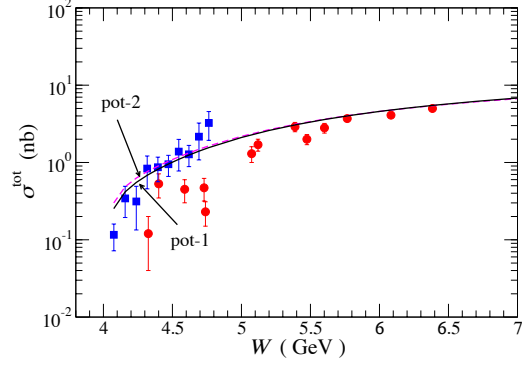


Fig. 14 The total cross sections of $\gamma + p \rightarrow J/\Psi + p$. t^{Pom} (t^{pot}) indicates the cross sections calculated from keeping only t^{Pom} (t^{pot}) term in Eq. (38). $t^{\text{Pom}} + t^{\text{pot}}$ indicate the cross sections calculated from the total amplitude.

In the upper part of Fig. 15, we see that the fit to the JLab total cross section data by using pot-2 is similar to that from pot-1. In the lower part, we see that the both models give equally good descriptions of the differential cross sections. The Pom-pot model can describe the data from threshold to very high energies of $W = 300$ GeV. Hence it can be used to predict the cross sections of J/Ψ photo-production from nuclei for investigating the production of nuclei with hidden charms [5–9], the gluon distributions in nuclei, and the nucleon-nucleon short-range correlations as discussed in Ref. [109].

4 Models of PQCD

In this section, we give the formulas for using GPD-based (Fig. 4) and $2g + 3g$ (Fig. 5) models within the formulation defined by Eqs. (27)–(30).

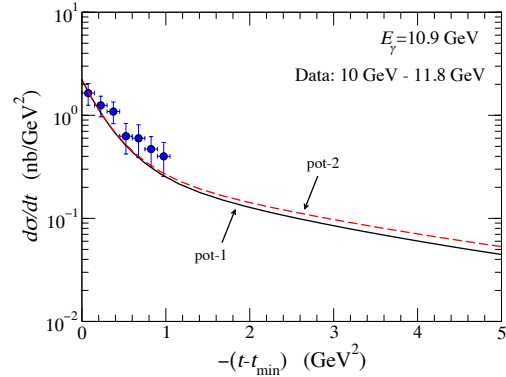


Fig. 15 Cross sections of $\gamma + p \rightarrow J/\Psi + p$ from using LQCD potentials pot-1 and pot-2. Upper: total cross sections; Lower: differential cross sections.

4.1 $2g + 3g$ model

The amplitudes of the $2g + 3g$ model, as defined by Eqs. (8)–(9), can be written as [9]

$$\langle \mathbf{k}, \lambda_{J/\Psi} m'_s | T_{J/\Psi N, \gamma N}(W) | \mathbf{q}, \lambda_\gamma m_s \rangle = \langle \mathbf{k}, \lambda_{J/\Psi} m'_s | t^{2g+3g}(W) | \mathbf{q}, \lambda_\gamma m_s \rangle, \quad (45)$$

where by defining the four-momenta as $k = (E_{J/\Psi}(\mathbf{k}), \mathbf{k})$, $p_f = (E_N(\mathbf{k}), -\mathbf{k})$, $q_i = (q, \mathbf{q})$, $p_i = (E_N(\mathbf{q}), -\mathbf{q})$, the amplitude can be written as

$$\begin{aligned} & \langle \mathbf{k}, \lambda_{J/\Psi} m'_s | t^{2g+3g}(W) | \mathbf{q}, \lambda_\gamma m_s \rangle \\ &= \frac{1}{(2\pi)^3} \sqrt{\frac{m_N m_N}{4E_{J/\Psi}(\mathbf{k}) E_N(\mathbf{p}_f) |\mathbf{q}| E_N(\mathbf{p}_i)}} \frac{4\sqrt{\pi} q W}{\sqrt{6} m_N} [M_{2g} + M_{3g}] \end{aligned} \quad (46)$$

with

$$M_{2g} = \frac{A_{2g}}{4\sqrt{\pi} R m_{J/\Psi}} e^{bt/2}, \quad (47)$$

$$M_{3g} = \frac{A_{3g}}{4\sqrt{\pi} R^2 m_{J/\Psi}^2} e^{bt/2}, \quad (48)$$

$$x = \frac{2m_N m_{J/\Psi} + m_{J/\Psi}^2}{W^2 - m_p^2}, \quad (49)$$

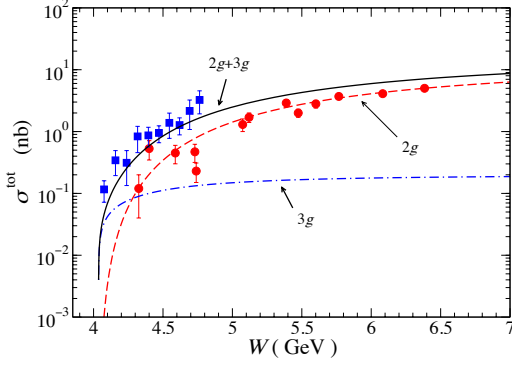


Fig. 16 Total cross sections of $\gamma + p \rightarrow J/\Psi + p$ calculated from $2g + 3g$ model. $2g$ ($3g$) is the contribution from two-gluon (three-gluon) exchange amplitudes of Eq. (46).

where $R = 1$ fm, $b = 1.13$ GeV $^{-2}$ are taken from Ref. [50]. Substituting Eqs. (45)-(46) into Eq. (28), we obtain

$$\frac{d\sigma_{J/\Psi N, \gamma N}}{d\Omega} = \frac{qk}{\pi} \left[\frac{d\sigma_{2g}}{dt} + \frac{d\sigma_{3g}}{dt} + C \times [2M_{2g}M_{3g}] \right], \quad (50)$$

where $\frac{d\sigma_{2g}}{dt}$ and $\frac{d\sigma_{3g}}{dt}$ are identical to those given in Eqs. (8) and (9), and C is a kinematic factor. The term $C \times [2M_{2g}M_{3g}]$ is from the interference between the amplitudes M_{2g} of $2g$ -exchange and M_{3g} of $3g$ -exchange. This term makes our approach slightly different from Ref. [50]. This modification is necessary for our later study of N^* in which the N^* interference with the non-resonant amplitudes is crucial.

We follow Ref. [50] to determine the parameters A_{2g} and A_{3g} by fitting the total cross section data. As shown in Fig. 16, we find the old data (solid circles) can be fitted by the two-gluon exchange ($2g$) model (dashed curve) with ($A_{2g} = 0.023$ MeV $^{-2}$, $A_{3g} = 0$). The JLab data can be fitted (solid curve) by adding the $3g$ exchange contribution (dash-dot curve) with ($A_{2g} = 0.028$ MeV $^{-2}$ and $A_{3g} = 2000$ MeV $^{-2}$).

The main difference between the *Pom*-DL model and the $2g + 3g$ model is at high energies, as shown in the upper part of Fig. 17. It remains to be explored whether the $2g + 3g$ model can be improved to also fit the data at high energies. Their difference can also be distinguished in differential cross sections at large t , as illustrated in the lower part of Fig. 17. Clearly more precise data are needed to test the predictions.

4.2 GPD-based model

In this subsection, we explain the derivations of the cross section in Eq. (6) from Eq. (5) within the *GPD*-based model. It is convenient to perform the calculation of the amplitude of $\gamma(q) + p(P) \rightarrow J/\Psi(K) + p(P')$ in the CM frame within

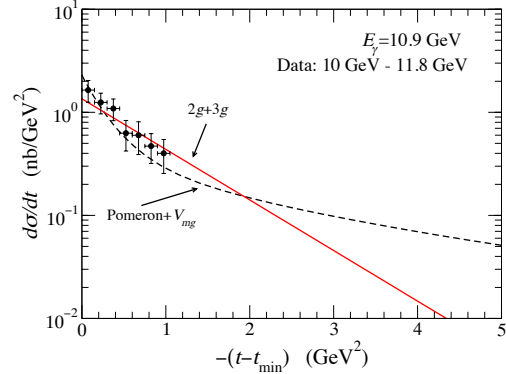
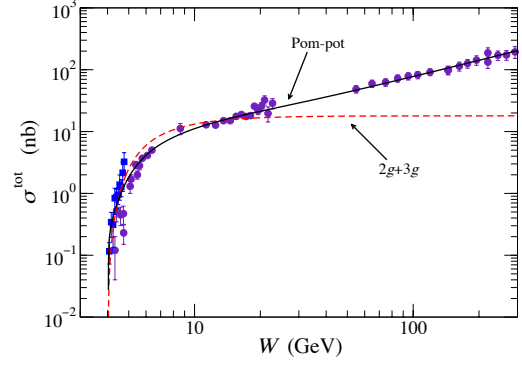


Fig. 17 Comparisons of the cross sections from *Pom*-DL and $2g + 3g$ models. Upper: total cross sections, Lower: differential cross sections.

which the initial nucleon momentum \mathbf{P} is in the z -direction and the final nucleon in the x - z plane:

$$\begin{aligned} P &= (P^0, 0, 0, |\mathbf{P}|), \\ q &= (q^0, 0, 0, -|\mathbf{P}|), \\ P' &= (P'^0, |\mathbf{P}'| \sin \theta, 0, |\mathbf{P}'| \cos \theta), \\ K &= (K^0, -|\mathbf{P}'| \sin \theta, 0, -|\mathbf{P}'| \cos \theta), \end{aligned}$$

where θ is the angle between \mathbf{P}' and z -axis. The skewness ξ is then defined by

$$\xi = -\frac{\Delta \cdot n}{2\bar{P} \cdot n}, \quad (51)$$

where $\Delta = P' - P$, and the light-cone vector n is defined as $n \equiv \frac{1}{\sqrt{2P^+}}(1, \mathbf{0}_\perp, -1)$ with the average nucleon momentum $\bar{P} \equiv (P + P')/2$ such that $n \cdot \bar{P} = 1$. We then have

$$\begin{aligned} \xi &= \frac{P^+ - P'^+}{P^+ + P'^+} \\ &= \frac{[E_N(\mathbf{P}) + |\mathbf{P}|] - [E_N(\mathbf{P}') + |\mathbf{P}'| \cos \theta]}{[E_N(\mathbf{P}) + |\mathbf{P}|] + [E_N(\mathbf{P}') + |\mathbf{P}'| \cos \theta]}, \end{aligned} \quad (52)$$

where $P^+ = \frac{1}{\sqrt{2}}(P^0 + P^3)$.

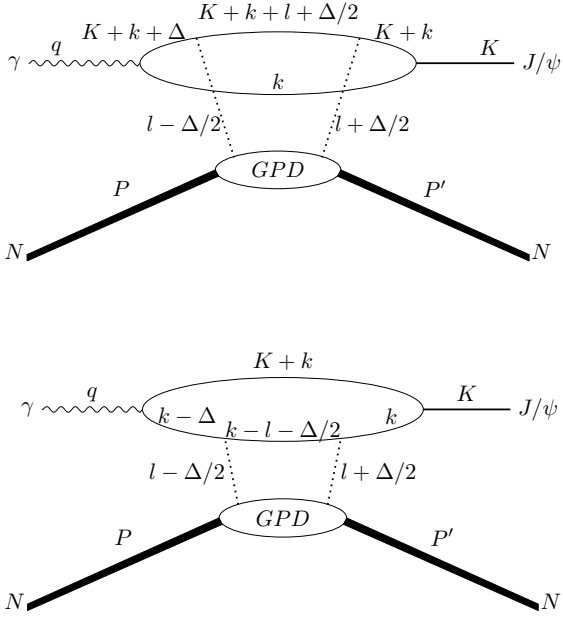


Fig. 18 The momentum variables of the two-gluon exchange amplitudes $I_{\mu\nu}^b$ (upper) and $I_{\mu\nu}^d$ (lower) of Eq. (53).

To illustrate the derivations of the formulas in Ref. [47], it is sufficient to only consider two of the four possible two-gluon-exchange amplitudes, as illustrated in Fig. 18. The amplitude can then be written as

$$t_{J/\Psi N, \gamma N}(P'K; Pq) = (ig)^2 \int \frac{d^4k d^4l}{(2\pi)^8} \langle P' | A^\mu(-l - \frac{\Delta}{2}) A^\nu(l - \frac{\Delta}{2}) | P \rangle \times \text{Tr} \left\{ \left[I_{\mu\nu}^b(K, k, l, \Delta, \epsilon_\gamma) + I_{\mu\nu}^d(K, k, l, \Delta, \epsilon_\gamma) \right] \Psi(K, k) \right\}, \quad (53)$$

where $\langle P' | A^\mu(-l - \frac{\Delta}{2}) A^\nu(l - \frac{\Delta}{2}) | P \rangle$ describes the distribution of the two exchanged-gluons in the nucleon, ϵ_γ is the photon polarization vector,

$$\Psi(K, k) = \langle \Psi_K | T \{ \psi_c(k) \bar{\psi}_c(K+k) \} | 0 \rangle \quad (54)$$

is the $c\bar{c}$ wavefunction of J/Ψ , and

$$I_b^{\mu\nu} = \gamma^\mu \frac{i}{\not{K} + \not{k} + \not{l} + \not{\Delta}/2 - m_c + i\epsilon} \gamma^\nu \times \frac{i}{\not{K} + \not{k} + \not{\Delta} - \not{\Delta}/2 - m_c + i\epsilon} \not{\epsilon}_\gamma, \quad (55)$$

$$I_d^{\mu\nu} = \not{\epsilon}_\gamma \frac{i}{\not{k} - \not{\Delta} - m_c + i\epsilon} \gamma^\nu \frac{i}{\not{k} - \not{l} - \not{\Delta}/2 - m_c + i\epsilon} \gamma^\mu \quad (56)$$

are the quark propagators in Fig. 18.

The calculations of Eqs. (53)-(56) are simplified by using the following approximations :

1. Use the threshold kinematics that the final J/Ψ and nucleon are at rest to simplify the loop integration over quark propagators by setting

$$\Delta \sim -(m_V, 0, 0, m_V/2), \quad (57)$$

$$l \sim x(m_V/2, 0, 0, m_V/2), \quad (58)$$

where $-1 \leq x \leq +1$ is the average momentum fraction of the two exchanged gluons.

2. Use a non-relativistic approximation to write

$$\begin{aligned} \Psi(K, k) &\sim \frac{u(k)\bar{v}(K+k)}{2E_c(k)} \tilde{\phi}(k) \\ &\rightarrow \frac{1}{4}(1 - \beta_V) \frac{1}{\sqrt{2}} \epsilon_V(1 + \beta_V) \\ &\quad \times (2\pi)^4 \delta^{(4)}(k + K/2) \phi_{NR}(0), \end{aligned} \quad (59)$$

where $\beta_V \equiv K/m_V$ and the non-relativistic wavefunction at relative distance between two quarks $r = 0$ is given by $\phi_{NR}(0)$.

3. Taking the light front gauge $A^+ = 0$, only A^\perp of the gluon field contributes to the leading twist. Therefore, only the terms with μ, ν in the transverse direction are kept in the calculation of Eq. (53).

By using Eqs. (57)-(59), Eq. (53) becomes

$$t_{J/\Psi N, \gamma N}(P'K; Pq) = (ig)^2 \phi_{NR}(0) \times \int \frac{d^4l}{(2\pi)^4} \langle P' | A^\mu(-l - \frac{\Delta}{2}) A^\nu(l - \frac{\Delta}{2}) | P \rangle \times 2 \frac{1}{\sqrt{2}m_c^2} [g^{\mu\nu}(\epsilon_\gamma \cdot \epsilon_V) + \epsilon_\gamma^\nu \epsilon_V^\mu - \epsilon_\gamma^\mu \epsilon_V^\nu]_\perp, \quad (60)$$

where the \perp subscript indicates that only the transverse components are non-zero.

By using the amplitude of Eq. (60), the differential cross section can be written as

$$\frac{d\sigma}{dt} = \frac{\alpha_{EM} e_Q^2}{4(W^2 - m_N^2)^2} \frac{(16\pi\alpha_S)^2}{3m_{J/\Psi}^3} |\phi_{NR}(0)|^2 |G(t, \xi)|^2, \quad (61)$$

where

$$G(t, \xi) = \frac{1}{2\xi} \int_{-1}^{+1} dx \left[\frac{1}{x + \xi - i\epsilon} - \frac{1}{x - \xi + i\epsilon} \right] \times F_g(x, \xi, t). \quad (62)$$

Here we have followed the standard definition of gluon GPD,

$$F_g(x, \xi, t) = \frac{1}{(\bar{P}^+)^2} \int \frac{d\lambda}{2\pi} e^{i\lambda x} \times \langle P' | \text{Tr} \{ F^{+i}(-\frac{\lambda n}{2}) F_i^+(-\frac{\lambda n}{2}) \} | P \rangle, \quad (63)$$

where we have defined in terms of gluon field A^μ of Eq. (53)

$$\begin{aligned} &\frac{1}{(\bar{P}^+)^2} [F^{+i}(-\frac{\lambda n}{2}) F_i^+(-\frac{\lambda n}{2})] \\ &= (x + \xi) A^i(-\frac{\lambda n}{2})(x - \xi) A_i(-\frac{\lambda n}{2}). \end{aligned} \quad (64)$$

Expanding the propagators in Eq. (62) as

$$\begin{aligned} &\frac{1}{2\xi} \left[\frac{1}{x + \xi - i\epsilon} - \frac{1}{x - \xi + i\epsilon} \right]_{\epsilon \rightarrow 0} \\ &= \frac{1}{2\xi} \frac{1}{\xi} \left[\left(1 + \frac{x}{\xi} \right)^{-1} + \left(1 - \frac{x}{\xi} \right)^{-1} \right] \\ &= \frac{1}{2\xi} \frac{1}{\xi} \left[\left(1 - \frac{x}{\xi} + \frac{x^2}{\xi^2} - \dots \right) + \left(1 + \frac{x}{\xi} + \frac{x^2}{\xi^2} - \dots \right) \right] \\ &= \frac{1}{\xi^2} \left[1 + \left(\frac{x}{\xi} \right)^2 + \dots \right], \end{aligned} \quad (65)$$

$G(t, \xi)$ is then expressed in terms of the even moments of the GPDs,

$$G(t, \xi) = \sum_{n=0}^{\infty} G^{(n)}(t, \xi) \quad (66)$$

with

$$G^{(n)}(t, \xi) = \frac{1}{\xi^{2n+2}} \int_{-1}^{+1} dx x^{2n} F_g(x, \xi, t). \quad (67)$$

The GPD defined by Eq. (63) is parameterized as

$$F_g(x, \xi, t) = \frac{1}{2\bar{P}^+} \left[H_g(x, \xi, t) \bar{u}(P') \gamma^+ u(P) + E_g(x, \xi, t) \bar{u}(P') \frac{i\sigma^{\alpha\Delta} \Delta_\alpha}{2M_N} u(P) \right]. \quad (68)$$

Keeping only the $n = 0$ moment, we then have

$$\begin{aligned} |G(t, \xi)|^2 &\rightarrow |G^{(0)}(t, \xi)|^2 \\ &= \frac{1}{\xi^4} \left[\left(1 - \frac{t}{4M_N^2} \right) E_2^2(t, \xi) \right. \\ &\quad \left. - 2E_2(x, \xi)(H_2(x, \xi) + E_2(x, \xi)) \right. \\ &\quad \left. + (1 - \xi^2)(H_2(x, \xi) + E_2(x, \xi))^2 \right], \quad (69) \end{aligned}$$

where

$$H_2(x, \xi) = \int_0^1 dx H_g(x, \xi, t) = A_g(t) + (2\xi)^2 C_g(t),$$

$$E_2(x, \xi) = \int_0^1 dx E_g(x, \xi, t) = B_g(t) - (2\xi)^2 C_g(t). \quad (70)$$

To use the results from the LQCD calculation of Ref. [49], one chooses the following dipole parameterization:

$$A_g(t) = \frac{A_g(0)}{\left(1 - \frac{t}{m_A^2}\right)^2}, \quad (71)$$

$$C_g(t) = \frac{C_g(0)}{\left(1 - \frac{t}{m_c^2}\right)^2}, \quad (72)$$

$$B_g(t) \sim 0 \quad (73)$$

with

$$m_A = 1.13 \text{ GeV}, \quad m_c = 0.48 \text{ GeV}, \quad (74)$$

$$A_g(0) = 0.58, \quad C_g(0) = -1.0. \quad (75)$$

To fit the JLab data, the above parameters were changed in Ref. [47] as $m_A = 1.13 \rightarrow (1.64 \pm 0.11)$ and $C_q(0) = -1 \rightarrow (-0.84 \pm 0.82)$. The results are in Fig. 19.

4.3 Holog model

The derivations of the *Holog* model by using the holographic approach can be found in Refs. [53, 54]. Here we only give the formulas of Ref. [54] which are used to calculate the cross sections for comparing with the JLab data and making predictions for future experimental tests.

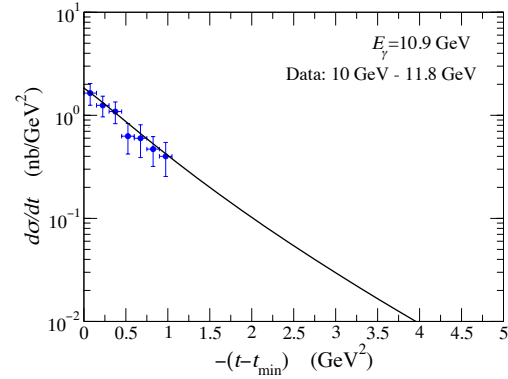
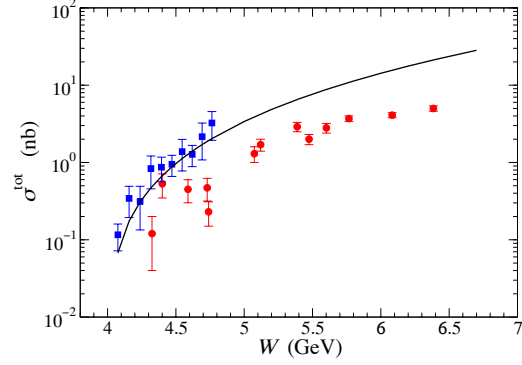


Fig. 19 GPD-based model. Upper: total cross sections, Lower: differential cross sections.

Within the *Holog* model, the $\gamma + N \rightarrow J/\Psi + N$ reaction is due to the exchange of scalar (0^{++}) and tensor (2^{++}) glueballs as illustrated in Fig. 6. The resulting expression of the differential cross sections is of the following form:

$$\begin{aligned} \frac{d\sigma}{dt} &= [A^2(0) \times \tilde{N}] I^2 N_T \left(\frac{s}{\tilde{\kappa}_N^2} \right)^2 \left(-\frac{t}{4m_N^2} + 1 \right) \\ &\quad \times \left[\frac{1}{(1 - t/\Lambda_t^2)^2} \right]^2, \quad (76) \end{aligned}$$

where $\Lambda_t = 1.124 \text{ GeV}$, and

$$I = \frac{3 g_5 f_{J/\Psi}}{2 M_{J/\Psi}} \times \left[\frac{1}{\left(\frac{Q^2}{4\tilde{\kappa}_{J/\Psi}^2} + 3 \right) \left(\frac{Q^2}{4\tilde{\kappa}_{J/\Psi}^2} + 2 \right) \left(\frac{Q^2}{4\tilde{\kappa}_{J/\Psi}^2} + 1 \right)} \right]_{Q^2=0} \quad (77)$$

$$N_T = \frac{1}{64\pi} \left[e^2 \frac{(2\kappa^2)^2}{g_5^2} \right] \frac{\tilde{\kappa}_N^4}{\tilde{\kappa}_{J/\Psi}^8} \quad (78)$$

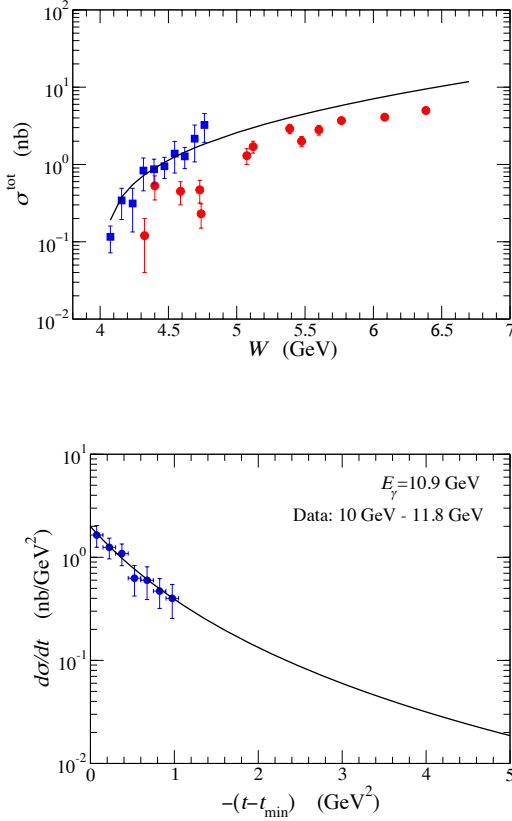


Fig. 20 Holog model. Upper: total cross sections; Lower: differential cross sections.

with

$$g_5 = \frac{2^{3/2} \tilde{\kappa}_{J/\Psi}^2}{f_{J/\Psi} m_{J/\Psi}}, \quad (79)$$

$$\kappa = \sqrt{4\pi^2 / N_c^2}. \quad (80)$$

The parameters in the above equations are: $N_c = 3$, $e = 0.3$, $\tilde{\kappa}_N = 0.35$, $m_N = 0.94$ GeV, $m_{J/\Psi} = 3.1$ GeV, $f_{J/\Psi} = 0.405$ GeV, and $\tilde{\kappa}_{J/\Psi} = 1.03784$ GeV. The normalization constant $[A^2(0) \times \tilde{N}]$ is fixed by fitting the JLab data,

$$A^2(0) \times \tilde{N} = 43.11 \mu\text{b}/\text{GeV}^2. \quad (81)$$

The total cross section is then obtained by

$$\sigma^{\text{tot}}(s) = \int_{|t|_{\min}}^{|t|_{\max}} dt \frac{d\sigma}{dt}. \quad (82)$$

The results are compared with the JLab data in Fig. 20.

5 N^* excitation

To study the $N^*(P_c)$ in $\gamma + p \rightarrow J/\Psi + p$, we first note that there are coupled-channel effects due to the couplings between $J/\Psi N$, ρN , πN and multi-meson XN channels. These

coupled-channel effects were studied in Ref. [110] and were found to be small. Hence Eqs. (11) and (12) are sufficient for the calculations presented below.

Since the width of $N^*(P_c)$ is very narrow ~ 20 MeV, we can assume $M_{N^*} + \Sigma_{N^*}(E) \sim M_R - \frac{i}{2}\Gamma^{\text{tot}}(W)$, and Eq. (12) then becomes the usual Breit-Wigner form. In the CM system, the amplitude of $\gamma(\mathbf{q}, \lambda_\gamma) + N(-\mathbf{q}, \lambda_N) \rightarrow N^*(J, M_J) \rightarrow J/\Psi(\mathbf{k}, m_{J/\Psi}) + N(-\mathbf{k}, m'_s)$ can then be written as

$$\begin{aligned} \langle \mathbf{k}, m_{J/\Psi} m'_s | t_{JM_J}^{N^*} | \mathbf{q}, \lambda_\gamma \lambda_N \rangle &= \langle \mathbf{k}, m_{J/\Psi} m'_s | \bar{F}_{N^*, J/\Psi N} | JM_J \rangle \\ &\times \frac{1}{W - M_R + \frac{i}{2}\Gamma^{\text{tot}}(W)} \langle JM_J | F_{N^*, \gamma N}^\dagger | \mathbf{q}, \lambda_\gamma \lambda_N \rangle, \end{aligned} \quad (83)$$

where λ_γ and λ_N are the helicities of the photon and the incoming nucleon, respectively, $m_{J/\Psi}$ and m'_s are the spin projections of the J/Ψ and the recoiled nucleon. The spin and its projection of the intermediate N^* are denoted by J and M_J , respectively.

Following Ref. [72], the matrix element of the $\gamma N \rightarrow N^*$ transition is

$$\begin{aligned} \langle JM_J | F_{N^*, \gamma N}^\dagger | \mathbf{q}, \lambda_\gamma \lambda_N \rangle &= \delta_{\lambda, (\lambda_\gamma - \lambda_N)} \frac{1}{(2\pi)^{3/2}} \sqrt{\frac{m_N q_{N^*}}{E_N(q)}} \\ &\times A_\lambda D_{\lambda, M_J}^J(\phi_q, \theta_q, -\phi_q), \end{aligned} \quad (84)$$

where A_λ is the helicity amplitude of the $\gamma N \rightarrow N^*$ excitation, q_{N^*} and q are determined by $M_R = q_{N^*} + E_N(q_{N^*})$ and $W = q + E_N(q)$, respectively, and

$$D_{\lambda, M_J}^J(\phi_q, \theta_q, -\phi_q) = e^{i(\lambda - M_J)\phi} d_{\lambda, M_J}^J(\theta_q). \quad (85)$$

Here $d_{\lambda, M_J}^J(\theta_q)$ is the Wigner d -function.

The matrix element of the $N^* \rightarrow J/\Psi N$ transition is parameterized [72] as

$$\begin{aligned} \langle \mathbf{k}, m_{J/\Psi} m'_s | \bar{F}_{N^*, J/\Psi N} | JM_J \rangle &= \sum_{LS} \sum_{M_L M_S} \langle JM_J | LSM_L M_S \rangle \langle SM_S | 1 \frac{1}{2} m_{J/\Psi} m_s \rangle Y_{LM_L}(\hat{\mathbf{k}}) \\ &\times \frac{1}{(2\pi)^{3/2}} \frac{1}{\sqrt{2E_{J/\Psi}(k)}} \sqrt{\frac{m_N}{E_N(k)}} \sqrt{\frac{8\pi^2 M_R}{m_N k}} G_{LS}^J \left(\frac{k}{k_{N^*}} \right)^L, \end{aligned} \quad (86)$$

where k and k_{N^*} are determined by $W = E_{J/\Psi}(k) + E_N(k)$ and $M_R = E_{J/\Psi}(k_{N^*}) + E_N(k_{N^*})$, and L and S are the orbital angular momentum and total spin of the J/Ψ - N system. $\langle j m | j_1 m_1 j_2 m_2 \rangle$ is the Clebsch-Gordan coefficient, and $Y_{LM_L}(\hat{\mathbf{k}})$ is the spherical harmonic function. We follow the dynamical approach of Ref. [72] to define the W -dependence of $\Gamma^{\text{tot}}(W)$ in Eq. (83) as

$$\Gamma^{\text{tot}}(W) = \Gamma_0^{\text{tot}} \frac{\rho(k)}{\rho(k_{N^*})} \left(\frac{k}{k_{N^*}} \right)^{2L} \left(\frac{\Lambda^2}{(k - k_{N^*})^2 + \Lambda^2} \right)^{2L+4}, \quad (87)$$

where $\rho(k) = \pi k E_N(k) E_{J/\Psi}(k) / (E_N(k) + E_{J/\Psi}(k))$ and $\Lambda = 650$ MeV is a cutoff parameter.

The resonance amplitude of Eq. (83) then have parameters: the total decay width Γ_0^{tot} , helicity amplitude A_λ for $N^* \rightarrow \gamma N$ of Eq. (84), and G_{LS} for $N^* \rightarrow J/\Psi N$ of Eq. (86). These parameters can be related to the partial decay widths defined by

$$\begin{aligned} \Gamma_{N^*, \gamma N} &= \int d\mathbf{q} \delta(M_R - E_N(\mathbf{q}) - |\mathbf{q}|) \\ &\times \frac{2\pi}{2J+1} \sum_{M_J} \sum_{\lambda_\gamma \lambda_N} |\langle \mathbf{q}, \lambda_\gamma \lambda_N | \bar{F}_{N^*, \gamma N}^\dagger | JM_J \rangle|^2 \\ &= \frac{q_{N^*}^2 m_N}{4\pi M_R} \frac{8}{2J+1} (|A_{1/2}|^2 + |A_{3/2}|^2), \end{aligned} \quad (88)$$

and

$$\begin{aligned} \Gamma_{N^*, J/\Psi N} &= \int d\mathbf{k} \delta(M_R - E_{J/\Psi}(\mathbf{k}) - E_N(\mathbf{k})) \\ &\times \frac{2\pi}{2J+1} \sum_{M_J} \sum_{m_{J/\Psi} m'_s} |\langle \mathbf{k}, m_{J/\Psi} m'_s | \bar{F}_{N^*, J/\Psi N}^\dagger | JM_J \rangle|^2 \\ &= \sum_{LS} |G_{LS}^J|^2. \end{aligned} \quad (89)$$

Our objective here is to investigate the extent to which the available JLab data can be related to the $P_c(4337)$ state reported recently by the LHCb Collaboration [4]. We will assume that the non-resonant amplitude in Eq. (11) is defined by the amplitude generated from either the *Pom*-pot or $2g + 3g$ models described in the previous sections. The spin-parity of $P_c(4337)$ state was not well determined and has four possible specifications. For our illustrative purposes, it is sufficient to only consider $J^\pi(LS) = \frac{1}{2}^+(0, 1)$, $\frac{3}{2}^+(2, 1)$, and use their values of decay widths $\Gamma^{\text{tot}} = 29$ MeV and $\Gamma_{N^*, J/\Psi N} = 6.8$ MeV. For simplicity, we set $A_{3/2} = 0$ and hence $A_{1/2}$ is the only parameter in fitting the JLab data.

We first consider the specification $J^\pi(LS) = \frac{1}{2}^+(0, 1)$. We find that the total cross section calculated with $A_{1/2} \lesssim 1 \times 10^{-3} \text{ GeV}^{-2}$ are within the uncertainties of the available data. Our results with $A_{1/2} = 1 \times 10^{-3} \text{ GeV}^{-2}$ and $A_{3/2} = 0$ are shown in Fig. 21. At the resonance energy $W = M_R = 4.337$ GeV, the results from *Pom*-pot and $2g - 3g$ models are almost the same, indicating that our determination of $A_{1/2}$ is rather model independent. It appears that the available JLab data can not unambiguously exclude or confirm the $P_c(4337)$ state of LHCb.

We next consider $J^\pi(LS) = \frac{3}{2}^+(2, 1)$. We find that by also setting the helicity amplitude $A_{1/2} = 1 \times 10^{-3} \text{ GeV}^{-2}$ and $A_{3/2} = 0$, the total cross sections are almost indistinguishable with that of $J^\pi(LS) = \frac{1}{2}^+(0, 1)$. However their differential cross sections are rather different at large $|t|$, as shown in Fig. 22. The cross sections for $J^\pi(LS) = \frac{3}{2}^+(2, 1)$ raise at large t can be a clear signal for identifying this N^* state.

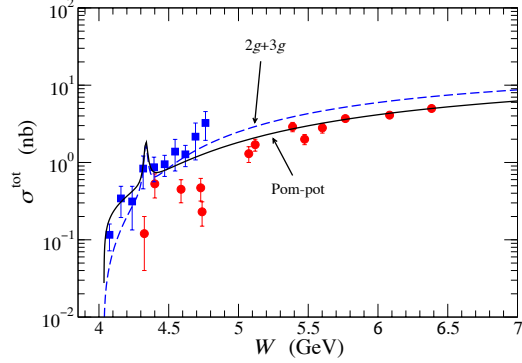


Fig. 21 Fits to the total cross section data of $\gamma + p \rightarrow J/\Psi + p$. The $P_c(4337)$ ($J^\pi(LS) = \frac{1}{2}^+(0, 1)$, $A_{1/2} = 1 \times 10^{-3} \text{ GeV}^{-2}$) is included in the fits with the non-resonant amplitudes calculated from either the *Pom*-pot (solid curve) or $2g + 3g$ (dashed curve) models.

6 *Pom*-CQM model

In this section we describe the *Pom*-CQM model which can be used to relate the J/Ψ -N potentials extracted from LQCD calculation [45, 108] to the $\gamma + p \rightarrow J/\Psi + p$ cross sections. It is obtained by removing the VMD assumption within the *Pom*-pot model and using the CQM to evaluate the $c\bar{c}$ -loop mechanisms, illustrated in the upper part of Fig. 7. Since the resulting model is also applicable to heavy quark system Y , we will use the notation V for J/Ψ in this section.

We start with the following Hamiltonian,

$$H = H_0 + H_{\text{em}} + v_{c\bar{c}} + v_{cN}, \quad (90)$$

where H_0 is the free Hamiltonian, $v_{c\bar{c}}$ is a quark-quark potential of CQM, v_{cN} is a quark-nucleon potential, and the electromagnetic $\gamma \rightarrow e^+e^-$, $c\bar{c}$ couplings are defined by

$$\begin{aligned} H_{\text{em}} &= e \int dx \bar{\psi}_e(x) \gamma^\mu \psi_e(x) A_\mu(x) \\ &+ e_c \int dx \bar{\psi}_c(x) \gamma^\mu \psi_c(x) A_\mu(x), \end{aligned} \quad (91)$$

where $\psi_e(x)$ and $\psi_c(x)$ are the field operators of the electron with charge e and the charm quark with charge e_c , respectively.

With the quark-quark potential $v_{c\bar{c}}$ in the Hamiltonian of Eq. (90), we can generate the J/Ψ wavefunction $|\phi_V\rangle$ in the rest frame of J/Ψ by solving the following bound-state equation,

$$(H_0 + v_{c\bar{c}}) |\phi_V\rangle = E_V |\phi_V\rangle, \quad (92)$$

where E_V is the mass of J/Ψ . The wavefunction ϕ_V can then be used to define J/Ψ -N potential $V_{VN, VN}$ from v_{cN} by using the folding procedure [111]:

$$V_{VN, VN} = \langle \phi_V, N | \sum_c v_{cN} | \phi_V, N \rangle. \quad (93)$$

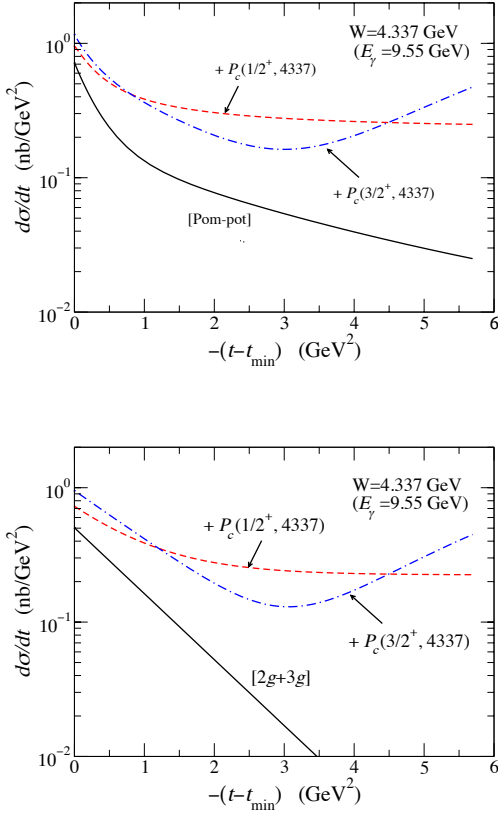


Fig. 22 The effects of the resonance $P_c(4337)$ on the differential cross sections of $\gamma + p \rightarrow J/\Psi + p$. The non-resonant amplitudes are calculated from *Pom-pot* (Upper) or $2g+3g$ (Lower) models. The results from adding the resonance amplitude are the curves indicated by $+P_c(\frac{1}{2}^+, 4337)$ and $+P_c(\frac{3}{2}^+, 4337)$.

The J/Ψ photo-production is also defined by the quark-nucleon potential v_{cN} as

$$B_{VN,\gamma N} = \langle \phi_V, N | \left[\sum_c v_{cN} \right] \frac{|c\bar{c}\rangle \langle c\bar{c}|}{E_{c\bar{c}} - H_0} f_{\gamma, c\bar{c}} | \gamma, N \rangle, \quad (94)$$

where $f_{\gamma, c\bar{c}}$ is the $\gamma \rightarrow c\bar{c}$ coupling defined by the Hamiltonian H_{em} of Eq. (91), and $E_{c\bar{c}}$ is the energy available to the propagation of $c\bar{c}$.

The unitarity condition requires the final state interaction (FSI) of the outgoing VN and hence the total $\gamma + N \rightarrow J/\Psi + N$ amplitude defined by the Hamiltonian of Eqs. (90) and (91) is

$$t_{VN,\gamma N}^{\text{CQM}}(W) = B_{VN,\gamma N} + t_{VN,\gamma N}^{(\text{fsi})}(W), \quad (95)$$

where

$$t_{VN,\gamma N}^{(\text{fsi})}(W) = T_{VN,VN}(W) \frac{1}{W - H_0 + i\epsilon} B_{VN,\gamma N}. \quad (96)$$

Here $T_{VN,VN}(W)$ is the $VN \rightarrow VN$ scattering amplitude calculated from $V_{VN,VN}$ defined in Eq. (93) by solving the following Lippmann-Schwinger equation,

$$T_{VN,VN}(W) = V_{VN,VN} + V_{VN,VN} \frac{1}{W - H_0 + i\epsilon} T_{VN,VN}(W) \quad (97)$$

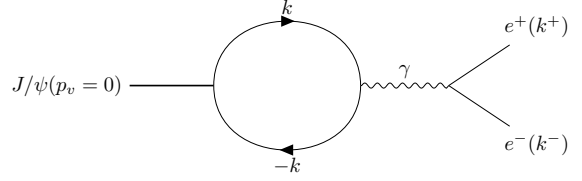


Fig. 23 Momentum variables of $J/\Psi \rightarrow e^+e^-$ decay in the rest frame of J/Ψ .

In order to fit the data from threshold to $W = 300$ GeV, the Pomeron-exchange amplitude is included to define the total amplitude of *Pom-CQM* model as

$$T_{VN,\gamma N}(W) = t_{VN,\gamma N}^{\text{Pom}}(W) + t_{VN,\gamma N}^{\text{CQM}}(W), \quad (98)$$

where $t_{VN,\gamma N}^{\text{Pom}}(W)$ has been given in Sec. 2. To be consistent, we should calculate $t_{VN,\gamma N}^{\text{Pom}}$ by also using CQM to calculate the $c\bar{c}$ -loop illustrated in the lower part of Fig. 7. This will require adjusting the Pomeron-quark parameters to fit the high energy data, as shown in Fig. 9, and is beyond the scope of this work. Taking into account the spin indices and momentum variables, we now give detailed formula for calculating the above equations in the following subsections.

6.1 Determination of the J/Ψ wavefunction

For this exploratory study, we will not generate the J/Ψ wavefunction from solving Eq. (92) within a CQM. Instead we will assume a simple s -wave wavefunction,

$$\phi_{\mathbf{p}_V, M_V}(\mathbf{k}_1 m_{s_q}, \mathbf{k}_2 m_{s_{\bar{q}}}) = \delta(\mathbf{p}_V - \mathbf{k}_1 - \mathbf{k}_2) \times \langle J_V M_V | \frac{1}{2} \frac{1}{2} m_{s_q} m_{s_{\bar{q}}} \rangle \phi(\mathbf{k}), \quad (99)$$

where \mathbf{p}_V is the momentum of J/Ψ , \mathbf{k}_i is the momentum of the i -th quark, $\mathbf{k} = \frac{\mathbf{k}_1 - \mathbf{k}_2}{2}$, $J_V M_V$ is the total angular momentum of J/Ψ , m_{s_q} and $m_{s_{\bar{q}}}$ are the spins of quarks c and \bar{c} , respectively. We assume a simple Gaussian form

$$\phi(\mathbf{k}) = N_0 e^{-\mathbf{k}^2/b^2}, \quad (100)$$

where N_0 is determined by the normalization condition,

$$\int d\mathbf{k} \phi^*(\mathbf{k}) \phi(\mathbf{k}) = 1. \quad (101)$$

The amplitude of $J/\Psi \rightarrow c(\mathbf{k}) + \bar{c}(-\mathbf{k}) \rightarrow \gamma \rightarrow e^+(\mathbf{k}_e) + e^-(-\mathbf{k}_e)$ in the rest frame of J/Ψ with $\mathbf{p}_V = 0$, as illustrated in Fig. 23, is of the following form:

$$\langle k_+ m_{s_+} k_- m_{s_-} | T | \phi_{\mathbf{p}_V, M_V} \rangle = \frac{e}{(2\pi)^3} \left[\bar{u}_{m_{s_+}}(\mathbf{k}_e) \gamma_\mu v_{m_{s_-}}(-\mathbf{k}_e) \right] \times \frac{1}{m_V^2} F_{M_V}^\mu, \quad (102)$$

where $k_+ = (E_e(\mathbf{k}_e), \mathbf{k}_e)$, $k_- = (E_e(\mathbf{k}_e), -\mathbf{k}_e)$, and

$$F_{M_V}^\mu = e_c \sum_{m_{s_q}, m_{s_{\bar{q}}}} \int d\mathbf{k} \frac{m_c}{E_c(\mathbf{k})} \left[\bar{v}_{m_{s_{\bar{q}}}}(\mathbf{k}) \gamma^\mu u_{m_{s_q}}(-\mathbf{k}) \right] \times \langle J_V M_V | \frac{1}{2} \frac{1}{2} m_{s_q} m_{s_{\bar{q}}} \rangle \phi(\mathbf{k}). \quad (103)$$

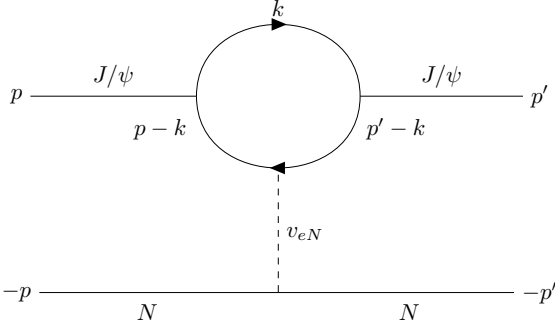


Fig. 24 Momentum variables for the calculation of $V_{VN,VN}$ defined by Eq. (106).

Here $e_c = \frac{2}{3}e$ is the charge of c quark. The decay width of $J/\Psi \rightarrow e^+e^-$ is then calculated from

$$\begin{aligned} \Gamma_{V \rightarrow e^+e^-} &= (2\pi) \int d\mathbf{k} \delta(m_V - 2E_e(\mathbf{k}_e)) \\ &\times \sum_{m_{s_+} m_{s_-}} \frac{1}{2J_V + 1} \sum_{M_V} |\langle k_+ m_{s_+} k_- m_{s_-} | T | \phi_{\mathbf{p}\mathbf{V}, M_V} \rangle|^2 \\ &= \frac{k_e}{(2\pi)^5} \frac{1}{m_V^5} \left(\frac{2}{3} e^2 \right)^2 \\ &\times \frac{1}{2J_V + 1} \sum_{M_V} A^{\mu\nu}(k_+, k_-) F_{M_V, \mu} F_{M_V, \nu}^* \end{aligned} \quad (104)$$

with

$$A^{\mu\nu}(k_+, k_-) = k_+^\mu k_-^\nu + k_+^\nu k_-^\mu - g^{\mu\nu}(k_+ \cdot k_- + m_e^2). \quad (105)$$

With the above formulas, the parameter b of the J/Ψ wavefunction defined by Eqs. (99) and (100) is determined by fitting the data of $J/\Psi \rightarrow e^+e^-$ decay. We find that the decay width $\Gamma_{J/\Psi \rightarrow e^+e^-} = 5.1$ keV can be reproduced with $b = 2.5$ GeV.

6.2 J/Ψ -N potential

To evaluate Eq. (93), we assume for simplicity that quark-nucleon interaction, v_{cN} , is independent of spin variables,

$$\begin{aligned} \langle \mathbf{k} m_{s_c}, \mathbf{p} m_{s_N} | v_{cN} | \mathbf{k}' m'_{s_c}, \mathbf{p}' m'_{s_N} \rangle &= \delta_{m_{s_c}, m'_{s_c}} \delta_{m_{s_N}, m'_{s_N}} \\ &\times \delta(\mathbf{k} + \mathbf{p} - \mathbf{k}' - \mathbf{p}') \langle \mathbf{q} | v_{cN} | \mathbf{q}' \rangle, \end{aligned} \quad (106)$$

where the relative momenta are defined by

$$\mathbf{q} = \frac{m_N \mathbf{k} - m_c \mathbf{p}}{m_N + m_c}, \quad (107)$$

$$\mathbf{q}' = \frac{m_N \mathbf{k}' - m_c \mathbf{p}'}{m_N + m_c}. \quad (108)$$

Here m_c and m_N are the masses of the quark c and the nucleon, respectively.

With the spin independent potential of Eq. (106) and the s -wave J/Ψ wavefunction of Eq. (99), the J/Ψ -N defined by Eq. (93) is also spin independent. In the CM frame, $\mathbf{k}_V = -\mathbf{p}$

and $\mathbf{k}'_V = -\mathbf{p}'$ as illustrated in Fig. 24, the matrix element of Eq. (93) can be written as

$$\begin{aligned} \langle \mathbf{k}_V m_V, \mathbf{p} m_s | V_{VN,VN} | \mathbf{k}'_V m'_V, \mathbf{p}' m'_s \rangle &= \delta_{m_V, m'_V} \delta_{m_s, m'_s} \\ &\times \delta(\mathbf{k}_V + \mathbf{p} - \mathbf{k}'_V - \mathbf{p}') \langle \mathbf{p} | V_{VN} | \mathbf{p}' \rangle, \end{aligned} \quad (109)$$

where

$$\begin{aligned} \langle \mathbf{p} | V_{VN} | \mathbf{p}' \rangle &= 2 \int d\mathbf{k} \phi^*(\mathbf{k} - \frac{\mathbf{p}}{2}) \\ &\times \left\langle \mathbf{p} - \frac{m_N}{m_N + m_c} \mathbf{k} \left| v_{cN} \right| \mathbf{p}' - \frac{m_N}{m_N + m_c} \mathbf{k} \right\rangle \\ &\times \phi(\mathbf{k} - \frac{\mathbf{p}'}{2}). \end{aligned} \quad (110)$$

Here the factor 2 is from summing the contributions from two quarks in J/Ψ , and we have used the definitions of Eqs. (107) and (108).

For simplicity, we choose a Yukawa form $v_{cN}(r) = \alpha \frac{e^{-\mu r}}{r}$ with r being the distance between two quarks. We then have

$$\left\langle \mathbf{p} - \frac{m_N}{m_N + m_c} \mathbf{k} \left| v_{cN} \right| \mathbf{p}' - \frac{m_N}{m_N + m_c} \mathbf{k} \right\rangle = v_{cN}(\mathbf{p} - \mathbf{p}') \quad (111)$$

where

$$\begin{aligned} v_{cN}(\mathbf{p} - \mathbf{p}') &= \frac{\alpha}{(2\pi)^3} \int d\mathbf{r} e^{i(\mathbf{p} - \mathbf{p}') \cdot \mathbf{r}} \left(\frac{\alpha e^{-\mu r}}{r} \right) \\ &= \frac{2\alpha}{(2\pi)^2} \frac{1}{(\mathbf{p} - \mathbf{p}')^2 + \mu^2}. \end{aligned} \quad (112)$$

By using Eq. (111), Eq. (110) becomes the following factorized form,

$$\langle \mathbf{p} | V_{VN} | \mathbf{p}' \rangle = F_V(\mathbf{t}) [2v_{cN}(\mathbf{t})], \quad (113)$$

where $\mathbf{t} = \mathbf{p} - \mathbf{p}'$ and

$$\begin{aligned} F_V(\mathbf{t}) &= \int d\mathbf{k} \phi^*(\mathbf{k} - \frac{\mathbf{p}}{2}) \phi(\mathbf{k} - \frac{\mathbf{p}'}{2}) \\ &= \int d\mathbf{k} \phi^*(\mathbf{k} - \frac{\mathbf{t}}{2}) \phi(\mathbf{k}) \end{aligned} \quad (114)$$

is the form factor of the vector meson V .

The J/Ψ -N potential defined in Eqs. (109)-(114) is then used to get scattering amplitude by solving Eq. (97). The resulting amplitude is spin independent and is

$$\begin{aligned} \langle \mathbf{p} m_V m_s | T_{VN,VN}(W) | \mathbf{p}' m'_V m'_s \rangle &= \delta_{m_V, m'_V} \delta_{m_s, m'_s} \\ &\times \left\langle \mathbf{p}' \left| T_{VN}(W) \right| \mathbf{p} \right\rangle, \end{aligned} \quad (115)$$

where $\langle \mathbf{p}' | T_{VN}(W) | \mathbf{p} \rangle$ is from solving

$$\begin{aligned} \langle \mathbf{p}' | T_{VN}(W) | \mathbf{p} \rangle &= \langle \mathbf{p}' | V_{VN} | \mathbf{p} \rangle \\ &+ \int d\mathbf{p}'' \langle \mathbf{p}' | V_{VN} | \mathbf{p}'' \rangle \frac{1}{W - E_N(p'') - E_V(p'') + i\epsilon} \\ &\times \langle \mathbf{p}'' | T_{VN}(W) | \mathbf{p} \rangle. \end{aligned} \quad (116)$$

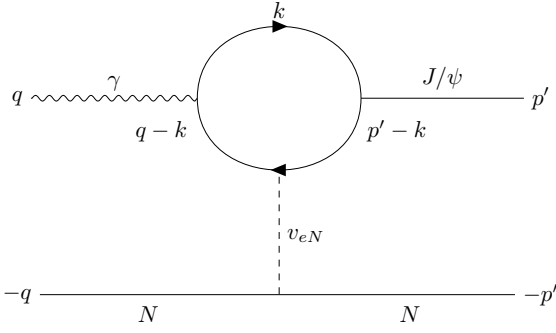


Fig. 25 Momentum variables for calculating the matrix element of photo-production of Eq. (117).

6.3 J/Ψ photo-production

By using Eq. (99) for the J/Ψ wave function and Eq. (106) for quark-N potential, the matrix element of photo-production of Eq. (94) can be calculated. With the variables in the CM system, as illustrated in Fig. 25, we follow the dynamical formulation of Refs. [71–74] to write

$$\begin{aligned}
& \langle \mathbf{p}' m_V m_s' | B_{VN, \gamma N} | \mathbf{q} \lambda m_s \rangle \\
&= \sum_{m_c, m_{\bar{c}}} \frac{1}{(2\pi)^3} \frac{e_c}{\sqrt{2|\mathbf{q}|}} \int d\mathbf{k} \langle J_V m_V | \frac{1}{2} \frac{1}{2} m_c, m_{\bar{c}} \rangle \phi(\mathbf{k} - \frac{1}{2} \mathbf{p}') \\
&\quad \times \delta_{m_s, m_s'} \left\langle \mathbf{p}' - \frac{m_N}{m_N + m_c} \mathbf{k} \left| v_{cN} \right| \mathbf{q} - \frac{m_N}{m_N + m_c} \mathbf{k} \right\rangle \\
&\quad \times \frac{1}{W - E_N(\mathbf{q}) - E_c(\mathbf{q} - \mathbf{k}) - E_c(\mathbf{k}) + i\epsilon} \\
&\quad \times \bar{u}_{m_q}(\mathbf{k}) [\epsilon_\lambda \cdot \boldsymbol{\gamma}] v_{m_{\bar{q}}}(\mathbf{q} - \mathbf{k}). \tag{117}
\end{aligned}$$

If we choose the same Yukawa form of v_{cN} of Eq. (111), we obtain the following factorized form:

$$\begin{aligned}
\langle \mathbf{p}' m_V m_s' | B_{VN, \gamma N} | \mathbf{q} \lambda m_s \rangle &= C_{\lambda, m_V} \delta_{m_s, m_s'} B(\mathbf{p}', \mathbf{q}) \\
&\quad \times [2v_{cN}(\mathbf{q} - \mathbf{p}')], \tag{118}
\end{aligned}$$

where

$$\begin{aligned}
B(\mathbf{p}', \mathbf{q}) &= \frac{1}{(2\pi)^3} \frac{e_c}{\sqrt{2|\mathbf{q}|}} \int d\mathbf{k} \phi(\mathbf{k} - \frac{1}{2} \mathbf{p}') \\
&\quad \times \frac{1}{W - E_N(\mathbf{q}) - E_c(\mathbf{q} - \mathbf{k}) - E_c(\mathbf{k}) + i\epsilon} \\
&\quad \times \sqrt{\frac{E_c(\mathbf{k}) + m_c}{2E_c(\mathbf{k})}} \sqrt{\frac{E_c(\mathbf{q} - \mathbf{k}) + m_c}{2E_c(\mathbf{q} - \mathbf{k})}} \\
&\quad \times \left(1 - \frac{\mathbf{k} \cdot (\mathbf{q} - \mathbf{k})}{[E_c(\mathbf{k}) + m_c][E_c(\mathbf{q} - \mathbf{k}) + m_c]} \right) \tag{119}
\end{aligned}$$

and

$$C_{\lambda, m_V} = \sum_{m_q, m_{\bar{q}}} \langle J_V m_V | \frac{1}{2} \frac{1}{2} m_q m_{\bar{q}} \rangle \langle m_{\bar{q}} | \boldsymbol{\sigma} \cdot \boldsymbol{\epsilon}_\lambda | m_q \rangle. \tag{120}$$

With Eqs. (115) and (117), the matrix element of Eq. (95) can be calculated as

$$\begin{aligned}
\langle \mathbf{p}' m_V m_s' | t_{VN, \gamma N}^{(\text{CQM})} | \mathbf{q} \lambda m_s \rangle &= \langle \mathbf{p}' m_V m_s' | B_{VN, \gamma N} | \mathbf{q} \lambda m_s \rangle \\
&\quad + \langle \mathbf{p}' m_V m_s' | t_{VN, \gamma N}^{(\text{fsi})} | \mathbf{q} \lambda m_s \rangle, \tag{121}
\end{aligned}$$

where

$$\begin{aligned}
& \langle \mathbf{p}' m_V m_s' | t_{VN, \gamma N}^{(\text{fsi})} | \mathbf{q} \lambda m_s \rangle \\
&= \sum_{m_V'', m_s''} \int d\mathbf{p}'' \langle \mathbf{p} m_V m_s' | T_{VN, VN} | \mathbf{p}'' m_V'', m_s'' \rangle \\
&\quad \times \frac{1}{W - E_N(p'') - E_V(p'') + i\epsilon} \\
&\quad \times \langle \mathbf{p}'' m_V'' m_s'' | B_{VN, \gamma N} | \mathbf{q} \lambda, m_s \rangle. \tag{122}
\end{aligned}$$

The total amplitude of Eq. (98) of the *Pom*-CQM model is then of the following form:

$$\begin{aligned}
\langle \mathbf{p}' m_V m_s' | T_{VN, \gamma N}^{\text{Pom-CQM}} | \mathbf{q} \lambda, m_s \rangle &= \langle \mathbf{p}' m_V m_s' | t_{VN, \gamma N}^{\text{Pom}} | \mathbf{q} \lambda, m_s \rangle \\
&\quad + \langle \mathbf{p}' m_V m_s' | t_{VN, \gamma N}^{\text{CQM}} | \mathbf{q} \lambda, m_s \rangle, \tag{123}
\end{aligned}$$

where $t_{VN, \gamma N}^{\text{Pom}}$ has been given in Sec. 2.

6.4 Results

We now turn to discussing the results from using Eq. (123). We first consider the case that $\langle \mathbf{p}' | V_{VN} | \mathbf{p} \rangle$ of Eq. (113) can be identified with the matrix element of J/Ψ -N potential extracted from LQCD shown in Fig. 13. It turns out that the form factor $F_V(\mathbf{t})$ drops from $F_V(0) = 1$ very slowly as momentum transfer t increases, and hence we can use the approximation $\langle \mathbf{p}' | V_{VN} | \mathbf{p} \rangle \sim 2v_{cN}(\mathbf{t})$ for Eq. (113). Thus the parameters of $v_{cN}(r)$ can be directly determined by the potentials *pot-1* and *pot-2* (Fig. 13) from LQCD.

We find that the FSI effects due to the $t_{VN, VN}^{(\text{fsi})}$ term in Eq. (121) are significant in increasing the total cross sections, as shown in the upper part of Fig. 26. However, the predicted magnitudes, from using the parameters of v_{cN} determined by using *pot-1* or *pot-2* in Fig. 13, are very small. When Pomeron-exchange is included, the JLab data can not be explained, as shown in the lower part of Fig. 26.

Since the LQCD calculation of Ref. [45] was a very first step, the results shown in Fig. 13 will certainly be revised by using more advanced LQCD calculations, such as those reported in Refs. [112, 113] for the spin-dependent J/Ψ -N potential and Ref. [114] for the ϕ -N potential. Thus we will determine the parameters α and μ of quark-N potential $v_{cN} = \alpha \frac{e^{-\mu r}}{r}$ by fitting the JLab data. The resulting parameters may be taken as the data to test future LQCD calculations. In the upper part of Fig. 27, we show the sensitivity to the parameter α and $\alpha = -0.25$ clearly is favored by the data at low energies. In the lower part of Fig. 27, we show the dependence on μ and $\mu = 0.3$ GeV seems favored by the data.

The best fit to JLab data is from using $\alpha = -0.25$ and $\mu = 0.3$ GeV. The contributions from each mechanism are shown in Fig. 28. The Born term $B_{VN, \gamma NN}$ (B) of *Pom*-CQM is larger than the Pomeron-exchange (t^{Pom}) near threshold.

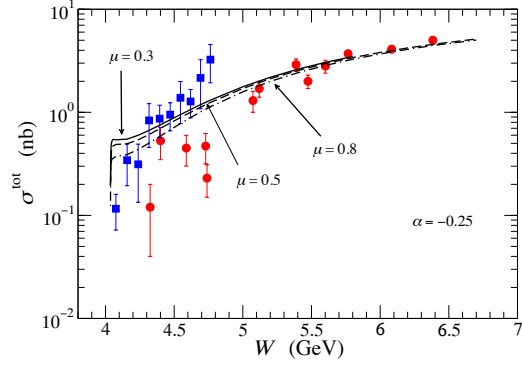
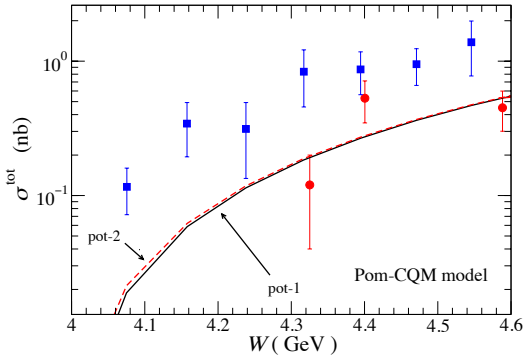
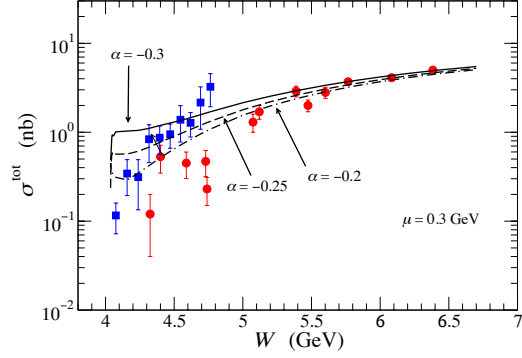
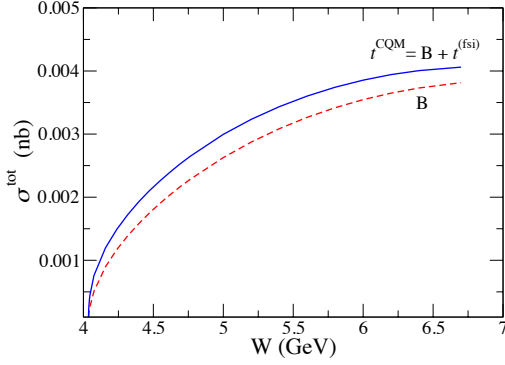


Fig. 26 *Pom-CQM* model. The results are from using the parameters of quark-nucleon potential v_{cN} determined from the J/Ψ -N potentials extracted from LQCD. Upper: effect of final-state interaction. Lower: Comparisons with JLab data. pot-1 (pot-2) indicates that the parameters of quark-nucleon potential v_{cN} are determined by using the potentials pot-1 (pot-2) extracted from LQCD shown in Fig. 13.

Fig. 27 Dependence of the total cross sections on the parameter α (upper) and β (lower) of the quark-nucleon potential $v_{cN} = \alpha \frac{e^{-\mu r}}{r}$ within the *Pom-CQM* model.

When the Pomeron-exchange is included ($t^{\text{Pom}}+B$), the predicted results are still below the Jlab data. Only when FSI effects are included ($t^{\text{Pom}} + B + t^{\text{fsi}}$), we obtain the black solid curve which agrees reasonably with the Jlab data. The pronounced enhancement due to FSI at very near threshold is similar to that seen in nuclear reactions. The predicted differential cross sections are comparable to that of the *Pom-pot* model in describing the Jlab data, as shown in Fig. 29.

Apparently, the results presented here need to be examined by using the J/Ψ wavefunction generated from a more realistic CQM which fits the spectrum of charmonium ($c\bar{c}$) and the width of $J/\Psi \rightarrow e^+e^-$ decay. Since the momentum-transfer for the $\gamma \rightarrow c\bar{c} \rightarrow J/\Psi$ loop (Fig. 24) and $J/\Psi \rightarrow c\bar{c} \rightarrow J/\Psi$ loop (Fig. 25) are rather different in the threshold region, the parameters for the quark-nucleon potential v_{cN} may have to be determined differently for these two calculations. It is, of course, most important to have new calculations of J/Ψ -N interaction from LQCD and the DSE models which can be tested within this reaction model.

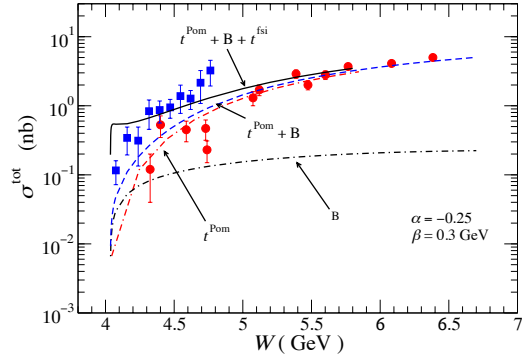


Fig. 28 Comparisons of the contribution from each amplitude in Eqs. (121)-(123).

7 Predictions

The available JLab data can be reasonably fitted by the six models presented in this paper. Their differences can only be tested by using more extensive data from the future experiments [11–13]. This can be seen in Fig. 30 for the differen-

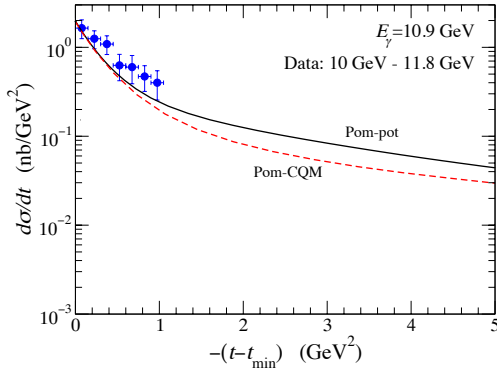


Fig. 29 Comparisons of differential cross sections from *Pom-pot* and *Pom-CQM* models.

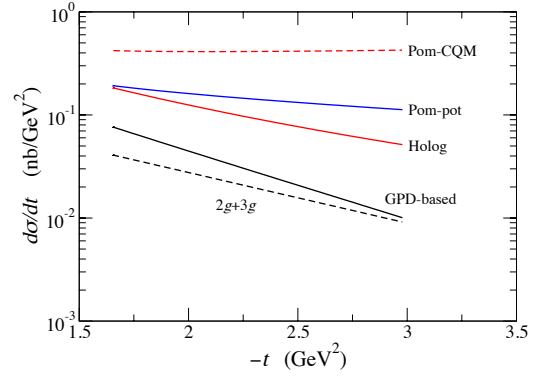


Fig. 31 Comparison of the differential cross sections at invariant mass $W = 4.056$ GeV predicted by the five models presented in this paper.

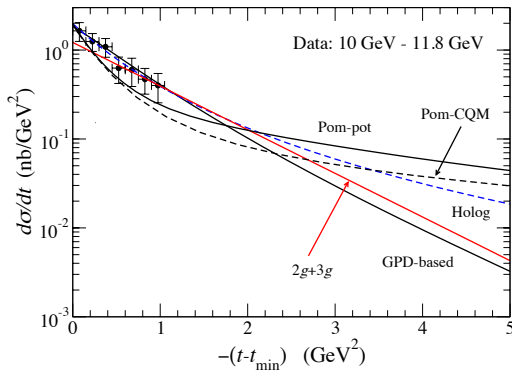


Fig. 30 Comparison of the differential cross sections from the five models presented in this paper.

tial cross sections at large $|t|$. Their differences become very dramatic at very near threshold, $W = 4.056$ GeV, as shown in Fig. 31.

For the search of N^* states, an effective way is to examine the energy-dependence of the differential cross sections at a given scattering angle θ . Our predictions for the $P_c(4337)$ state are given in Fig. 32. It will be interesting to see that these predictions and the t -dependence of differential cross sections, shown in Fig. 22, can be tested by the forthcoming data from JLab.

8 Summary and future developments

To facilitate the future study of the role of gluons in determining the structure of the nucleon and J/Ψ -nucleon (J/Ψ -N) interactions, we have reviewed six reaction models of $\gamma + p \rightarrow J/\Psi + p$ reactions. The formulas for each model are given and used to obtain the results to show the extent to which the available data can be described. The models

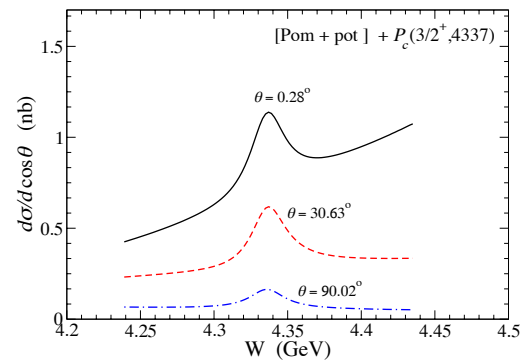
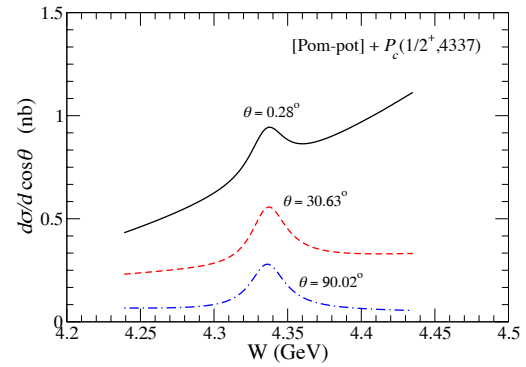


Fig. 32 The energy-dependence of the differential cross sections calculated from including the nucleon resonance $P_b(4337)$ with $J^\pi = \frac{1}{2}^+$ and $\frac{3}{2}^+$. θ is the scattering angle of the outgoing J/Ψ .

which have been developed to describe the data from threshold to very high energy $W = 300$ GeV are the Pomeron-exchange model of Donnachie and Landshoff (*Pom-DL*) and its extensions to include J/Ψ -N potentials extracted from LQCD (*Pom-pot*) and to also use the CQM to account for

the quark substructure of J/Ψ (*Pom*-CQM). For describing the JLab data at $W \lesssim 7$ GeV, three models have been developed by applying the PQCD approach to calculate the two-gluon exchange using the generalized parton distribution of the nucleon (*GPD*-based), two- and three-gluon exchanges using the parton distribution of the nucleon ($2g + 3g$), and the exchanges of scalar (0^{++}) and tensor (2^{++}) glueballs within the holographic formulation (*Holog*). The formulas for investigating the excitation of the nucleon resonances $N^*(P_c)$, reported by the LHCb Collaboration, in the $\gamma + N \rightarrow J/\Psi + N$ reactions have also been given. We demonstrate that the differences between these six models can be better distinguished and the N^* can be more precisely studied by using the forthcoming JLab data at large $-t$ and at energies very near the J/Ψ production threshold.

We have observed that all six models are still in developing stage. It will be useful to make the following improvements:

1. The *Pom*-DL and *Pom*-pot models need to replace the vector meson dominance assumption by the quark-loop mechanism using either the constituent quark model or the models based on Dyson-Schwinger equation of QCD. This is necessary to interpret the determined Pomeron-quark coupling constants.
2. *Pom*-CQM model needs to use realistic constituent quark models which fit both the charmonium spectrum and the $J/\Psi \rightarrow e^+e^-$ decay width, and to use a parameterization of quark-nucleon potential v_{cN} which account for the spin-dependent and momentum-dependent of the multi-gluon exchange mechanisms. It will be interesting to use the information from *GPD*-based model to constraint the parameters of v_{cN} . It is of course essential to have the input from the most advanced LQCD calculations of J/Ψ -N potential, such as those reported in Refs. [112, 113] for the spin-dependent J/Ψ -N potential and Ref. [114] for the ϕ -N potential. The J/Ψ -N interaction calculated from DSE models is also highly desirable.
3. Both the *GPD*-based and $2g + 3g$ models can be improved by using either CQM or DSE models to perform quark-loop integration over the J/Ψ wavefunction and to also predict J/Ψ -N scattering amplitudes which must be included to account for the final-state interaction of $\gamma + N \rightarrow J/\Psi + N$, as required by the unitarity condition.

By using the reaction models with the improvements suggested above, the analysis of the forthcoming JLab data can help determine the J/Ψ -N interaction which is needed to test J/Ψ -N potential extracted from lattice QCD and to understand the nucleon resonances $N^*(P_c)$ reported by the LHCb Collaboration. In addition, the determined J/Ψ -N potentials are also needed to investigate the production of nuclei with hidden charms and to extract the gluon distributions in nuclei. These goals can be accomplished by continu-

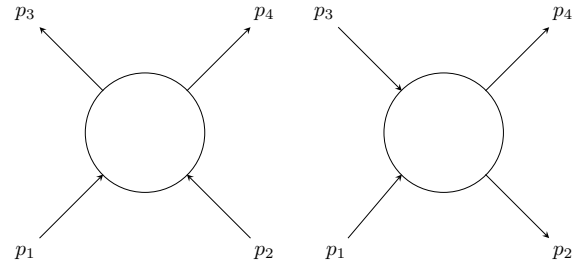


Fig. 33 Momentum variables of the s -channel (left) and t -channel scattering (right).

ing the collaborations between experimental and theoretical efforts.

Acknowledgements We are grateful to Shoichi Sasaki for providing the information on the J/Ψ -N potentials from LQCD of Refs. [45, 108] and to Craig Roberts for helpful discussions. We also thank Yuxun Guo and Kiminad Mamo for their help in checking the results from their models presented in this paper. The work of T.-S.H.L. was supported by the U.S. Department of Energy, Office of Science, Office of Nuclear Physics, under Contract No. DE-AC02-06CH11357. The work of S.S. and Y.O. was supported by the National Research Foundation of Korea (NRF) under Grants No. NRF-2020R1A2C1007597 and No. NRF-2018R1A6A1A06024970 (Basic Science Research Program).

Appendix A: Regge phenomenology

There exists extensive literature [14–16] on Regge phenomenology. For our purposes, we will only give sufficiently self-contained explanations which are needed to present the formulas of Pomeron-exchange models.

Considering the two-body scattering, the amplitudes of s -channel $1(p_1) + 2(p_2) \rightarrow 3(p_3) + 4(p_4)$ and t -channel $1(p_1) + 3(-p_3) \rightarrow 2(-p_2) + 4(p_4)$ scattering, as shown in Fig. 33, are written in terms of the usual Mandelstam variables defined by

$$s = (p_1 + p_2)^2, \quad (\text{A.1})$$

$$t = (p_1 - p_3)^2 \quad (\text{A.2})$$

for the s -channel scattering of Fig. 33(left) and

$$s_t = (p_1 + (-p_3))^2 = (p_1 - p_3)^2 = t, \quad (\text{A.3})$$

$$t_t = (p_1 - (-p_2))^2 = (p_1 + p_2)^2 = s \quad (\text{A.4})$$

for the t -channel of Fig. 33(right). One of the steps in developing Regge phenomenology is to assume the crossing symmetry that the scattering amplitudes $T(t, s)$ for the s -channel and $T_t(t_t, s_t)$ for the t -channel are related by

$$T(t, s) = T_t(s, t) = T_t(t_t, s_t). \quad (\text{A.5})$$

It is important to note here that s (s_t) is the total collision energy in the s -channel (t -channel) CM frame, and t (t_t) defines the corresponding momentum-transfer of the scattering. Thus the crossing symmetry implies that a bound or resonance state, called R , in the t -channel scattering $1 + 3 \rightarrow$

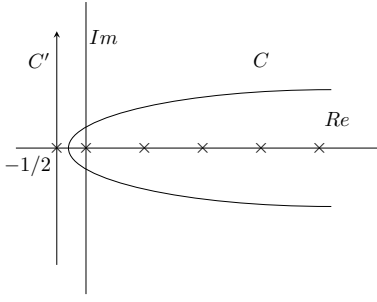


Fig. 34 Contour in l -plane.

$R \rightarrow 2 + 4$ can be an exchanged particle R in the s -channel $1 + 2 \rightarrow 3 + 4$ scattering.

We now describe the essential steps in getting the s -channel scattering amplitude $T(t, s)$ from the t -channel scattering amplitude $T_t(t, s_t)$ by using the crossing symmetry relation of Eq. (A.5). Considering $1(p_1) + 3(-p_3) \rightarrow 2(-p_2) + 4(p_4)$ in the CM system of the t -channel, we then have the following definitions of the momentum variables:

$$\begin{aligned} p &= |\mathbf{p}_1| = |\mathbf{p}_3|, \\ q &= |\mathbf{p}_2| = |\mathbf{p}_4|, \end{aligned} \quad (\text{A.6})$$

and

$$s_t = t = [E_1(p) + E_3(p)]^2 = [E_2(q) + E_4(q)]^2, \quad (\text{A.7})$$

$$t_t = s = m_1^2 + m_2^2 + 2E_1(p)E_2(q) - 2qp \cos \theta_t, \quad (\text{A.8})$$

where $\cos \theta_t = \hat{p}_1 \cdot (-\hat{p}_2)$ defines the scattering angle θ_t in t -channel. Eq. (A.8) then leads to

$$\cos \theta_t = \frac{1}{2pq} [s - m_1^2 - m_2^2 + 2E_1(p)E_2(q)]. \quad (\text{A.9})$$

Note that p and q are function of t as can be seen from Eq. (A.7) and hence for a given t , $\cos \theta_t$ depends linearly on s .

The next step is to examine the partial-wave expansion of t -channel amplitude. By using the relations Eqs. (A.7)-(A.9), we then have

$$\begin{aligned} T_t(t, s_t) &= T_t(t, \cos \theta_t, t) \\ &= \sum_{l=0}^{\infty} (2l+1) P_l(\cos \theta_t) A(l, t), \end{aligned} \quad (\text{A.10})$$

where $P_l(x)$ is a Legendre polynomial in x . In the complex- l plane, we apply the Watson-Sommerfeld transformation [115–117] to write the above expression as

$$\begin{aligned} T(t, s) &= T_t(t, s_t) \\ &= \frac{1}{2\pi i} \int_C \frac{\pi}{\sin l\pi} P_l(-\cos \theta_t) A(l, t) dl, \end{aligned} \quad (\text{A.11})$$

where C is the contour indicated in Fig. 34. The denominator $\sin l\pi$ generates the poles (solid circles) indicated in Fig. 34. Within the non-relativistic quantum mechanics, Regge [83–85] showed that if the s -channel amplitude $T(t, s)$ is defined by a local potential like Yukawa potential ($\sim e^{\mu r}/r$), $A(l, t)$

is analytic in the complex l -plane, aside from poles in the $\text{Re}(l) \geq -1/2$. It can therefore be written in the following form:

$$A(l, t) = \sum_n \frac{\beta_n(t)}{l - \alpha_n(t)}. \quad (\text{A.12})$$

Closing the contour C at infinity and through the $\text{Re}(J) = -1/2$ line, as indicated in Fig. 34, and using the Cauchy's theorem, Eq. (A.11) then becomes

$$\begin{aligned} T(t, s) &= T_t(t, s_t) \\ &= \int_{-1/2-i\infty}^{-1/2+i\infty} \frac{\pi}{\sin l\pi} P_l(-\cos \theta_t) A(l, t) dl \\ &\quad + \sum_n \beta_n(t) P_{\alpha_n(t)}(-\cos \theta_t) \frac{1}{\sin \pi \alpha_n(t)}. \end{aligned} \quad (\text{A.13})$$

Here $\alpha_n(t)$ is called the Regge trajectory which leads to poles of the amplitude at

$$\alpha_n(t = M_{L_n}^2) = L_n; \quad L_n = 0, 1, 2, \dots \quad (\text{A.14})$$

At these pole positions, the usual Legendre polynomial has the property $P_{\alpha_n(t)}(-\cos \theta) \rightarrow (-1)^{L_n} P_{L_n}(\cos \theta)$. Thus it is suggestive that L_n can be interpreted as the angular momentum of the particle formed in the t -channel process with mass M_{L_n} because $t = s_t = [E_1(p) + E_2(p)]^2$. These particles are interpreted as the exchanged particle in s -channel scattering. If this interpretation is correct, we can use the particle spectrum found in t -channel scattering to define the Regge trajectory. Thus the main feature of the Regge phenomenology is: **the particle spectrum can define the scattering amplitudes.**

The first term in Eq. (A.13) is neglected in practice. It is also extended to define natural-parity exchange from the unnatural-parity exchange. The amplitude of s -channel scattering amplitude is then of the following form:

$$T(s, t) = \sum_n \beta_n(t) \frac{P_{\alpha_n(t)}(-\cos \theta_t) + s_n P_{\alpha_n(t)}(+\cos \theta_t)}{2 \sin[\pi \alpha_n(t)]}, \quad (\text{A.15})$$

where the *signature* of the trajectory, $s_n = +1$ (-1) corresponds to even (odd) parity exchanges. In the high energy limit with very large s and $s \gg |t|$, $\cos \theta_t \sim -s/(2q(t)p(t))$, as can be seen from Eq. (A.9). It follows that

$$P_{\alpha_n(t)}(-\cos \theta_t) \sim \left(\frac{s}{2p(t)q(t)} \right)^{\alpha_n(t)}. \quad (\text{A.16})$$

Here we recall Eq. (A.7) to note that the momenta p and q of t -channel as functions of t of the s -channel scattering. We then have

$$T(s, t) = \sum_n F_t(t) \frac{1 + s_n e^{-i\pi \alpha_n(t)}}{2 \sin[\pi \alpha_n(t)]} [\alpha_{1,n}(t)s]^{\alpha_n(t)}, \quad (\text{A.17})$$

where

$$F_t(t) = \beta_n(t) \left(\frac{\alpha_{1,n}}{2p(t)q(t)} \right)^{-\alpha_n(t)}. \quad (\text{A.18})$$

If we write $F_f(t) = \beta_n^{13}(t)\beta_n^{24}(t)$ and assume that $\beta_n^{13}(t)$ and $\beta_n^{24}(t)$ characterize the hadron structure, we then have the following form

$$T(s,t) = \sum_n \beta_n^{13}(t)\beta_n^{24}(t) \frac{1 + s_n e^{-i\pi\alpha_n(t)}}{2 \sin[\pi\alpha_n(t)]} [\alpha_{1,n}(t)s]^{\alpha_n(t)}. \quad (\text{A.19})$$

The amplitude can then be interpreted as the exchange of particles with masses defined by $\alpha_n(t = M_{L_n}^2) = L_n$. This is an intuitively very attractive interpretation of the scattering. However, there exists no successful derivation of Eq. (A.19) from relativistic quantum field theory and the form factors $\beta_n^{13}(t)$ and $\beta_n^{24}(t)$ are determined experimentally or calculated from a theoretical model.

References

1. R. Aaij *et al.*, LHCb Collaboration, Observation of $J/\psi p$ resonances consistent with pentaquark states in $\Lambda_b^0 \rightarrow J/\psi K^- p$ decays, *Phys. Rev. Lett.* **115**, 072001 (2015).
2. R. Aaij *et al.*, LHCb Collaboration, Evidence for exotic hadron contributions to $\Lambda_b^0 \rightarrow J/\psi p \pi^-$ decays, *Phys. Rev. Lett.* **117**, 082003 (2016).
3. R. Aaij *et al.*, Observation of a narrow pentaquark state, $P_c(4312)^+$, and of the two-peak structure of the $P_c(4450)^+$, *Phys. Rev. Lett.* **122**, 222001 (2019).
4. R. Aaij *et al.*, LHCb Collaboration, Evidence for a new structure in the $J/\psi p$ and $J/\psi \bar{p}$ systems in $B_s^0 \rightarrow J/\psi p \bar{p}$ decays, *Phys. Rev. Lett.* **128**, 062001 (2022).
5. S. J. Brodsky, G. F. de Teramond, Spin correlations, QCD color transparency, and heavy-quark thresholds in proton-proton scattering, *Phys. Rev. Lett.* **60**, 1924 (1988).
6. S. J. Brodsky, I. Schmidt, G. F. de Teramond, Nuclear-bound quarkonium, *Phys. Rev. Lett.* **64**, 1011 (1990).
7. H. Gao, T.-S. H. Lee, V. Marinov, ϕ - N bound state, *Phys. Rev. C* **63**, 022201(R) (2001).
8. V. B. Belyaev, N. V. Shevchenko, A. Fix, W. Sandhas, Binding of charmonium with two- and three-body nuclei, *Nucl. Phys. A* **780**, 100 (2006).
9. J.-J. Wu, T.-S. H. Lee, Photoproduction of bound states with hidden charm, *Phys. Rev. C* **86**, 065203 (2012).
10. A. Ali *et al.*, GlueX Collaboration, First measurement of near-threshold J/ψ exclusive photoproduction off the proton, *Phys. Rev. Lett.* **123**, 072001 (2019).
11. Z.-E. Meziani *et al.*, A search for the LHCb charmed ‘pentaquark’ using photo-production of J/ψ at threshold in Hall C at Jefferson Lab, [arXiv:1609.00676](https://arxiv.org/abs/1609.00676).
12. A. Asaturyan *et al.*, A search for the LHCb charmed ‘pentaquark’ using photoproduction of J/ψ at threshold in Hall C at Jefferson Lab, Proposal to JLab-PAC44, PR12-16-007, 2016.
13. J. Arrington *et al.*, Near threshold electroproduction of J/ψ at 11 GeV, Proposal to JLab-PAC39, PR12-12-006, 2012.
14. P. D. B. Collins, *An Introduction to Regge Theory and High Energy Physics* (Cambridge Univ. Press, Cambridge, England, 1977).
15. A. C. Irving, R. P. Worden, Regge phenomenology, *Phys. Rep.* **34**, 117 (1977).
16. S. Donnachie, G. Dosch, P. Landshoff, O. Nachtmann, *Pomeron Physics and QCD* (Cambridge University Press, 2002).
17. M. Derrick *et al.*, ZEUS Collaboration, Measurement of the cross section for the reaction $\gamma p \rightarrow J/\psi p$ with the ZEUS detector at HERA, *Phys. Lett. B* **350**, 120 (1995).
18. D. P. Barber *et al.*, Charged ρ photoproduction in the energy range 2.8 GeV – 4.8 GeV, *Z. Phys. C* **2**, 1 (1979).
19. A. Donnachie, P. V. Landshoff, Elastic scattering and diffraction dissociation, *Nucl. Phys. B* **244**, 322 (1984).
20. A. Donnachie, P. V. Landshoff, Total cross sections, *Phys. Lett. B* **296**, 227 (1992).
21. A. Donnachie, P. V. Landshoff, Exclusive vector meson production at HERA, *Phys. Lett. B* **348**, 213 (1995).
22. A. Donnachie, P. V. Landshoff, Small x : two pomerons!, *Phys. Lett. B* **437**, 408 (1998).
23. J. J. Sakurai, Theory of strong interactions, *Ann. Phys. (N.Y.)* **11**, 1 (1960).
24. M. Gell-Mann, F. Zachariasen, Form factors and vector mesons, *Phys. Rev.* **124**, 953 (1961).
25. J. J. Sakurai, Vector-meson dominance and high-energy electron-proton inelastic scattering, *Phys. Rev. Lett.* **22**, 981 (1969).
26. J. J. Sakurai, D. Schildknecht, Generalized vector dominance and inelastic electron-proton scattering, *Phys. Lett.* **40B**, 121 (1972).
27. F. E. Low, Model of the bare Pomeron, *Phys. Rev. D* **12**, 163 (1975).
28. S. Nussinov, Colored-quark version of some hadronic puzzles, *Phys. Rev. Lett.* **34**, 1286 (1975).
29. A. Donnachie, P. V. Landshoff, Gluon condensate and Pomeron structure, *Nucl. Phys. B* **311**, 509 (1989).
30. P. V. Landshoff, J. C. Polkinghorne, The dual quark-parton model and high energy hadronic processes, *Nucl. Phys. B* **32**, 541 (1971).
31. G. A. Jaroszkiewicz, P. V. Landshoff, Model for diffraction excitation, *Phys. Rev. D* **10**, 170 (1974).
32. J.-J. Wu, T.-S. H. Lee, B.-S. Zou, Nucleon resonances with hidden charm in γp reactions, *Phys. Rev. C* **100**,

- 035206 (2019).
33. T.-S. H. Lee, Pomeron-LQCD model of J/ψ photoproduction on the nucleon, [arXiv:2004.13934](#).
 34. S.-H. Kim, T.-S. H. Lee, S.-I. Nam, Y. Oh, Dynamical model of ϕ meson photoproduction on the nucleon and ^4He , *Phys. Rev. C* **104**, 045202 (2021).
 35. S. Aid *et al.*, H1 Collaboration, Elastic electroproduction of ρ and J/ψ mesons at large Q^2 at HERA, *Nucl. Phys. B* **468**, 3 (1996); **548**, 639(E) (1999).
 36. B. Gittelmann, K. M. Hanson, D. Larson, E. Loh, A. Silverman, G. Theodosiou, Photoproduction of the $\psi(3100)$ meson at 11 GeV, *Phys. Rev. Lett.* **35**, 1616 (1975).
 37. U. Camerini, J. G. Learned, R. Prepost, C. M. Spencer, D. E. Wisner, W. W. Ash, R. L. Anderson, D. M. Ritson, D. J. Sherden, C. K. Sinclair, Photoproduction of the ψ particles, *Phys. Rev. Lett.* **35**, 483 (1975).
 38. M. E. Peskin, Short-distance analysis for heavy-quark systems (I). Diagrammatics, *Nucl. Phys. B* **156**, 365 (1979).
 39. G. Bhanot, M. E. Peskin, Short-distance analysis for heavy-quark systems (II). Applications, *Nucl. Phys. B* **156**, 391 (1979).
 40. M. Luke, A. V. Manohar, M. J. Savage, A QCD calculation of the interaction of quarkonium with nuclei, *Phys. Lett. B* **288**, 355 (1992).
 41. S. J. Brodsky, G. A. Miller, Is J/ψ -nucleon scattering dominated by the gluonic van der Waals interaction?, *Phys. Lett. B* **412**, 125 (1997).
 42. A. B. Kaidalov, P. E. Volkovitsky, Heavy-quark interactions with nucleons and nuclei, *Phys. Rev. Lett.* **69**, 3155 (1992).
 43. N. Ishii, S. Aoki, T. Hatsuda, Nuclear force from lattice QCD, *Phys. Rev. Lett.* **99**, 022001 (2007).
 44. S. Aoki, T. Hatsuda, N. Ishii, Theoretical foundation of the nuclear force in QCD and its applications to central and tensor forces in quenched lattice QCD simulations, *Prog. Theor. Phys.* **123**, 89 (2010).
 45. T. Kawanai, S. Sasaki, Charmonium-nucleon potential from lattice QCD, *Phys. Rev. D* **82**, 091501(R) (2010).
 46. T. Kawanai, S. Sasaki, Charmonium-nucleon interaction from lattice QCD with 2 + 1 flavors of dynamical quarks, *AIP Conf. Proc.* **1388**, 640 (2011).
 47. Y. Guo, X. Ji, Y. Liu, QCD analysis of near-threshold photon-proton production of heavy quarkonium, *Phys. Rev. D* **103**, 096010 (2021).
 48. Y. Guo, private communications, (2022).
 49. P. E. Shanahan, W. Detmold, Gluon gravitational form factors of the nucleon and the pion from lattice QCD, *Phys. Rev. D* **99**, 014511 (2019).
 50. S. J. Brodsky, E. Chudakov, P. Hoyer, J. M. Laget, Photoproduction of charm near threshold, *Phys. Lett. B* **498**, 23 (2001).
 51. S. J. Brodsky, M. Burkardt, I. Schmidt, QCD constraints on the shape of polarized quark and gluon distributions, *Nucl. Phys. B* **441**, 197 (1995).
 52. E. L. Berger, S. J. Brodsky, Quark structure functions of mesons and the Drell-Tan process, *Phys. Rev. Lett.* **42**, 940 (1979).
 53. K. A. Mamo, I. Zahed, Diffractive photoproduction of J/ψ and Υ using holographic QCD: Gravitational form factors and GPD of gluons in the proton, *Phys. Rev. D* **101**, 086003 (2020).
 54. K. A. Mamo, I. Zahed, Electroproduction of heavy vector mesons using holographic QCD: From near threshold to high energy regimes, *Phys. Rev. D* **104**, 066023 (2021).
 55. Y.-Z. Xu, S.-Y. Chen, Z.-Q. Yao, D. Binosi, Z.-F. Cui, C. D. Roberts, Vector-meson production and vector meson dominance, *Eur. Phys. J. C* **81**, 895 (2021).
 56. C. D. Roberts and A. G. Williams, Dyson-Schwinger equations and their application to hadronic physics, *Prog. Part. Nucl. Phys.* **33**, 477 (1994).
 57. C. D. Roberts, Electromagnetic pion form factor and neutral pion decay width, *Nucl. Phys. A* **605**, 475 (1996).
 58. M. A. Pichowsky, T.-S. H. Lee, Pomeron-exchange and exclusive electroproduction of ρ -mesons in QCD, *Phys. Lett. B* **379**, 1 (1996).
 59. M. A. Pichowsky, T.-S. H. Lee, Exclusive diffractive processes and the quark substructure of mesons, *Phys. Rev. D* **56**, 1644 (1997).
 60. P. Maris, C. D. Roberts, π - and K -meson Bethe-Salpeter amplitudes, *Phys. Rev. C* **56**, 3369 (1997).
 61. L. Chang, Y.-X. Liu, C. D. Roberts, Dressed-quark anomalous magnetic moments, *Phys. Rev. Lett.* **106**, 072001 (2011).
 62. L. Chang, I. C. Cloët, C. D. Roberts, S. M. Schmidt, P. C. Tandy, Pion electromagnetic form factor at space-like momenta, *Phys. Rev. Lett.* **111**, 141802 (2013).
 63. S.-X. Qin, C. D. Roberts, Impressions of the continuum bound state problem in QCD, *Chinese Phys. Lett.* **37**, 121201 (2020).
 64. Z.-Q. Yao, D. Binosi, Z.-F. Cui, C. D. Roberts, Semileptonic transitions: $B_{(s)} \rightarrow \pi(K)$; $D_s \rightarrow K$; $D \rightarrow \pi, K$; and $K \rightarrow \pi$, *Phys. Lett. B* **824**, 136793 (2022).
 65. R. Alkofer, L. von Smekal, The infrared behavior of QCD Green's functions. Confinement, dynamical symmetry breaking, and hadrons as relativistic bound states, *Phys. Rep.* **353**, 281 (2001).
 66. H. Sanchis-Alepuz, G. Eichmann, S. Villalba-Chávez, R. Alkofer, Delta and Omega masses in a three-quark covariant Faddeev approach, *Phys. Rev. D* **84**, 096003 (2011).
 67. G. Eichmann, C. S. Fischer, Unified description of hadron-photon and hadron-meson scattering in the

- Dyson-Schwinger approach, *Phys. Rev. D* **85**, 034015 (2012).
68. N. Isgur, G. Karl, Positive-parity excited baryons in a quark model with hyperfine interactions, *Phys. Rev. D* **19**, 2653 (1979).
 69. J.-M. Richard, An introduction to the quark model, [arXiv:1205.4326](https://arxiv.org/abs/1205.4326), talk at Ferrara International School Niccolò Cabeo 2012: Hadronic spectroscopy.
 70. J. Segovia, D. R. Entem, F. Fernandez, E. Hernandez, Constituent quark model description of charmonium phenomenology, *Int. J. Mod. Phys. E* **22**, 1330026 (2013).
 71. T. Sato, T.-S. H. Lee, Meson-exchange model for πN scattering and $\gamma N \rightarrow \pi N$ reaction, *Phys. Rev. C* **54**, 2660 (1996).
 72. A. Matsuyama, T. Sato, T.-S. H. Lee, Dynamical coupled-channel model of meson production reactions in the nucleon resonance region, *Phys. Rep.* **439**, 193 (2007).
 73. B. Juliá-Díaz, T.-S. H. Lee, A. Matsuyama, T. Sato, Dynamical coupled-channels model of πN scattering in the $W \leq 2$ GeV nucleon resonance region, *Phys. Rev. C* **76**, 065201 (2007).
 74. H. Kamano, S. X. Nakamura, T.-S. H. Lee, T. Sato, Nucleon resonances within a dynamical coupled-channels model of πN and γN reactions, *Phys. Rev. C* **88**, 035209 (2013).
 75. C.-W. Shen, F.-K. Guo, J.-J. Xie, B.-S. Zou, Disentangling the hadronic molecule nature of the $P_c(4380)$ pentaquark-like structure, *Nucl. Phys. A* **954** (2016).
 76. L. Roca, J. Nieves, E. Oset, LHCb pentaquark as a $\bar{D}^* \Sigma_c - \bar{D}^* \Sigma_c^*$ molecular state, *Phys. Rev. D* **92**, 094003 (2015).
 77. U.-G. Meißner, J. A. Oller, Testing the $\chi_{c1} p$ composite nature of the $P_c(4450)$, *Phys. Lett. B* **751**, 59 (2015).
 78. Y.-H. Lin, C.-W. Shen, F.-K. Guo, B.-S. Zou, Decay behaviors of the P_c hadronic molecules, *Phys. Rev. D* **95**, 114017 (2017).
 79. L. Maiani, A. D. Polosa, V. Riquer, The new pentaquarks in the diquark model, *Phys. Lett. B* **749**, 289 (2015).
 80. G.-N. Li, X.-G. He, M. He, Some predictions of diquark model for hidden charm pentaquark discovered at the LHCb, *JHEP* **2015**, 128 (2015).
 81. Z.-G. Wang, Analysis of $P_c(4380)$ and $P_c(4450)$ as pentaquark states in the diquark model with QCD sum rules, *Eur. Phys. J. C* **76**, 70 (2016).
 82. B. W. Lee, R. F. Sawyer, Regge poles and high-energy limits in field theory, *Phys. Rev.* **127**, 2266 (1962).
 83. T. Regge, Introduction to complex orbital momenta, *Nuovo Cim.* **14**, 951 (1959).
 84. T. Regge, Bound states, shadow states and Mandelstam representation, *Nuovo Cim.* **18**, 947 (1960).
 85. A. Bottino, A. M. Longoni, T. Regge, Potential scattering for complex energy and angular momentum, *Nuovo Cim.* **23**, 954 (1962).
 86. G. F. Chew, S-matrix theory of strong interactions without elementary particles, *Rev. Mod. Phys.* **34**, 394 (1962).
 87. G. F. Chew, S. C. Frautschi, Regge trajectories and the principle of maximum strength for strong interactions, *Phys. Rev. Lett.* **8**, 41 (1962).
 88. S. Mandelstam, Cuts in the angular-momentum plane I., *Nuovo Cim.* **30**, 1127 (1963).
 89. A. Donnachie, P. V. Landshoff, Elastic scattering at large t , *Z. Phys. C* **2**, 55 (1979).
 90. A. Donnachie, P. V. Landshoff, Multi-gluon exchange in pp elastic scattering, *Phys. Lett.* **123B**, 345 (1983).
 91. A. Donnachie, P. V. Landshoff, pp and $\bar{p}p$ elastic scattering, *Nucl. Phys. B* **231**, 189 (1984).
 92. I. Ia. Pomeranchuk, Equality of the nucleon and anti-nucleon total interaction cross section at high energies, *JETP* **34**, 499 (1958).
 93. M. L. Goldberger, K. M. Watson, *Collision Theory* (John Wiley and Sons, Inc., New York, 1964).
 94. Y. Oh, T.-S. H. Lee, One-loop corrections to ω photoproduction near threshold, *Phys. Rev. C* **66**, 045201 (2002).
 95. J. Breitweg *et al.*, ZEUS Collaboration, Measurement of elastic Y photoproduction at HERA, *Phys. Lett. B* **437**, 432 (1998).
 96. C. Adloff *et al.*, H1 Collaboration, Elastic photoproduction of J/ψ and Y mesons at HERA, *Phys. Lett. B* **483**, 23 (2000).
 97. S. Chekanov *et al.*, ZEUS Collaboration, Exclusive photoproduction of Y mesons at HERA, *Phys. Lett. B* **680**, 4 (2009).
 98. R. Aaij *et al.*, Measurement of Y production in pp collisions at $\sqrt{s} = 7$ TeV, *Eur. Phys. J. C* **72**, 2025 (2012).
 99. M. Derrick *et al.*, ZEUS Collaboration, Measurement of elastic ρ^0 photoproduction at HERA, *Z. Phys. C* **69**, 39 (1995).
 100. W. D. Shambroom *et al.*, Diffractive production of vector mesons in muon-proton scattering at 150 and 100 GeV, *Phys. Rev. D* **26**, 1 (1982).
 101. J. Ballam *et al.*, Vector-meson production by polarized photons at 2.8, 4.7, and 9.3 GeV, *Phys. Rev. D* **7**, 3150 (1973).
 102. W. Struczinski *et al.*, Aachen-Hamburg-Heidelberg-München Collaboration, Study of photoproduction on hydrogen in a streamer chamber with tagged photons for $1.6 \text{ GeV} < E_\gamma < 6.3 \text{ GeV}$: Topological and reaction cross sections, *Nucl. Phys. B* **108**, 45 (1976).
 103. R. M. Eglolf *et al.*, Measurements of elastic ρ^- - and ϕ -meson photoproduction cross sections on protons from 30 to 180 GeV, *Phys. Rev. Lett.* **43**, 657 (1979).

104. D. Aston *et al.*, Bonn-CERN-Ecole Polytechnique-Glasgow-Lancaster-Manchester-Orsay-Paris VI-Paris VII-Rutherford-Sheffield Collaboration, Photoproduction of ρ^0 and ω on hydrogen at photon energies of 20 to 70 GeV, *Nucl. Phys. B* **209**, 56 (1982).
105. M. Derrick *et al.*, ZEUS Collaboration, Measurement of elastic ϕ photoproduction at HERA, *Phys. Lett. B* **377**, 259 (1996).
106. H.-J. Behrend, J. Bodenkamp, W. P. Hesse, W. A. McNeely Jr., T. Miyachi, D. C. Fries, P. Heine, H. Hirschmann, A. Markou, E. Seitz, Elastic and inelastic ϕ photoproduction, *Nucl. Phys. B* **144**, 22 (1978).
107. Y. Oh, T.-S. H. Lee, ρ meson photoproduction at low energies, *Phys. Rev. C* **69**, 025201 (2004).
108. S. Sasaki, private communications, (2020).
109. Y. Hatta, M. Strikman, J. Xu, F. Yuan, Sub-threshold J/ψ and Υ production in γA collisions, *Phys. Lett. B* **803**, 135321 (2020).
110. J.-J. Wu, T.-S. H. Lee, Production of J/Ψ on the nucleon and on deuteron targets, *Phys. Rev. C* **88**, 015205 (2013).
111. H. Feshbach, *Theoretical Nuclear Physics: Nuclear Reactions* (John Wiley and Sons, Inc., New York, 1992).
112. T. Kawanai, S. Sasaki, Heavy quarkonium potential from Bethe-Salpeter wave function on the lattice, *Phys. Rev. D* **89**, 054507 (2014).
113. T. Kawanai, S. Sasaki, Potential description of charmonium and charmed-strange mesons from lattice QCD, *Phys. Rev. D* **92**, 094503 (2015).
114. Y. Lyu, T. Doi, T. Hatsuda, Y. Ikeda, J. Meng, K. Sasaki, T. Sugiura, Attractive N - ϕ interaction and two-pion tail from lattice QCD near physical point, [arXiv:2205.10544](https://arxiv.org/abs/2205.10544).
115. A. Sommerfeld, *Partial Differential Equations in Physics*, Pure and Applied Mathematics: A Series of Monographs and Textbooks Vol. 1 (Academic Press, 1949).
116. G. N. Watson, The diffraction of electric waves by the Earth, *Proc. Roy. Soc. Lond. A* **95**, 83 (1918).
117. G. N. Watson, The transmission of electric waves round the Earth, *Proc. Roy. Soc. Lond. A* **95**, 546 (1919).